Available online at www.sciencedirect.com
SCIENCE DIRECT®
International Journal of Heat and Mass Transfer 49 (2006) 1568–1591
International Journal of HEAT and MASS TRANSFER
www.elsevier.com/locate/ijhmt

A coupling model for macromolecule transport in a stenosed arterial wall

L. Ai, K. Vafai *

Department of Mechanical Engineering, University of California at Riverside, A363 Bourns Hall, Riverside, CA 92521-0425, USA

Received 11 July 2005; received in revised form 22 October 2005
Available online 21 February 2006

Abstract

A mathematical model is developed for the coupled analysis of the transport of macromolecules, such as low-density lipoproteins (LDL), in the blood stream and in the arterial walls. The advection–diffusion equations in porous media are used to model the species field in the arterial wall layers. The physical parameters needed are computed based on the available data from in vivo and in vitro measurements. The computed parameters are compared to those provided by other models and the differences are discussed. The advantage of the current model is that its set up is based on in vivo/vitro measurements and the calculated exact solutions of concentration field, leading to more reliable results. The model is used to simulate the LDL transport in a stenosed artery with various area reductions and stenosis numbers. The effects of hypertension and geometrical variation on the LDL accumulation within the wall are studied and discussed. This work provides essential information for studying atherogenesis.

1. Introduction

Atherosclerosis is a form of cardiovascular disease that is commonly located in the large- and medium-size arteries. The development of atherosclerosis is a complicated process which is associated with lipid deposition in the intima, intimal thickening, and smooth muscle cell (SMC) proliferation. Hence the transport of the low-density lipoprotein (LDL) from the blood into the arterial wall and its accumulation within the wall play an important role in the process of atherogenesis. The normal arterial wall can be divided into four layers, namely endothelium, intima, media and adventitia. As shown in Fig. 1, the innermost endothelium layer is lined by a monolayer of endothelial cells separating the blood from the vessel wall. The interendothelial junctions are typically 20 nm in width which are the primary pathway for many hydrophilic solutes.

The intima is considered to be an extracellular matrix of homogeneously distributed proteoglycan and collagen fibers. The thickened intima also contains the smooth muscle cells (SMCs). Equivalently, the media is modeled as a homogeneous porous medium composed of smooth muscle cells and elastic connective tissues. The intima and media are separated by the internal elastic lamina, which contains fenestral pores. The water and solutes are transported through the fenestral pores. In the large elastic artery, bands of elastin separate SMCs into several layers. However, they are not pronounced in the muscular artery and are not taken into account in our model. The adventitia is composed of fibrous tissue containing elastic fibers, lymphatics and the occasional nutrient vessels (vasa vasorum). It is widely accepted that the endothelium provides most of the resistance which regulates the transport of LDL into the arterial wall.

Computational modeling is an important avenue for better understanding of the physical factors that influence macromolecules transport process inside the biomedical systems. For example, the computational modeling is utilized to study the water molecules diffusion inside the brain extracellular space [1,2] and also for modeling detection of pathogens [3–6]. Several numerical and mathematical

* Corresponding author. Tel.: +1 951 827 2135; fax: +1 951 827 2899.
E-mail address: vafai@engr.ucr.edu (K. Vafai).

0017-9310/$ - see front matter © 2005 Elsevier Ltd. All rights reserved.
doi:10.1016/j.ijheatmasstransfer.2005.10.041

Nomenclature

A_{red}	area reduction
C	dimensional LDL concentration (mg/ml)
C_0	reference LDL concentration $C_0 = 1.2$ mg/ml
c	dimensionless LDL concentration, C/C_0
$\bar{c}$	volume-averaged LDL concentration
D	diffusivity of LDL (cm^2/s)
F	a function used in expressing inertia terms
J	a unit vector oriented along the velocity vector
k	the effective first-order reaction coefficient
K_D	Darcy permeability (cm^2)
L	thickness of a given artery wall layer (cm)
L_{un}	total length of the un-stenosed artery (cm)
L_{st}	total length of the stenosed artery (cm)
L_w	total thickness of the artery wall layer (cm)
n	unit vector normal to the interfaces
N_s''	mass flux of solute per unit area through the wall (cm/s)
p	hydraulic pressure (mm Hg)
P_{tot}	apparent permeability (cm/s)
P_{diff}	diffusive permeability (cm/s)
Pe	Peclet number
r	local radius (cm)
R_0	radius of the un-stenosed arterial lumen (cm)
R	hydraulic resistance (g/cm^2 s)
R_g	universal gas constant
Re	Reynolds number
t	dimensional time (s)
T	absolute temperature (K)
U_0	mean inlet velocity in the lumen (cm/s)
$\vec{u}$	velocity vector (cm/s)
u	dimensional axial velocity (cm/s)
u_{filt}	the filtration velocity through the wall (cm/s)
v	dimensional radial velocity (cm/s)
$w_{1,2}$	weighting functions
x_0	the stenosis half-length (cm)
x_{st}	the x coordinate of the center of the stenosis

Greek symbols

ν	kinematic viscosity (cm^2/s)
ρ	density (g/cm^3)
μ	dynamic viscosity of the whole blood (g/(cm s))
μ_p	dynamic viscosity of plasma (g/(cm s))
$\tilde{\mu}_p$	effective viscosity of plasma in a given medium (g/(cm s))
σ_d	the osmotic reflection coefficient
ε	porosity
τ	tortuosity
γ	the sieving coefficient
$\lambda_{1,2}$	the eigenvalues
ξ	ratio between the sieving coefficients of endothelium and IEL
κ	ratio between the diffusive permeabilities of endothelium and IEL
δ	dimensionless thickness of the luminal reduction in the radial direction

Subscripts

adv	adventitia
avg	mean value
eff	effective property
end	endothelium
iel	IEL
int	intima
l	lumen
med	media

models have been developed to study the LDL transport through the arterial walls [7–9]. According to the classification of Prosi et al. [10], there are usually three categories of the models depending on the level of description of the arterial wall. The wall-free model describes the arterial walls simply by means of some suitable boundary condition. Although this model requires a small number of parameters, the concentration profiles within the wall cannot be obtained [11]. The fluid–wall model approximates the wall structure by a simple homogeneous layer. It is better than the wall-free model. However, it is still quite inaccurate as it misses the major wall components which are crucial to atherosclerosis [8].

The multilayer model is the most complex model which takes into account the heterogeneous properties of the layers constituting the wall. Due to its complexity, a larger number of parameters are required to characterize the physical properties of each layer [7,12]. Most of the previous multilayer models are based on the assumption that the physical properties of the porous wall can be identified by the pore theory. However, this approach does not provide satisfactory estimations. Prosi et al. [10] proposed a new methodology which starts from a set of data that can be easily determined by experimental measurements. However, some of the assumptions made in this model give substantial errors. For example, the Kedem–Katchalsky equations used for endothelium and IEL do not take into account the boundary effects associated with the flow across these two layers. In fact, these effects are large due to the thickness of these two layers ($\sim$2 μm). Also, they take into account the effects of the reaction inside the media layer by approximating the loss of mass flux upstream of the layer. This simplification can lead to an over or underestimation of the influence of the chemical reaction. In addition, they obtain the value of diffusive permeability in the endothelium under the assumption of no convection flow which substantially overestimates the value of the diffusive permeability.

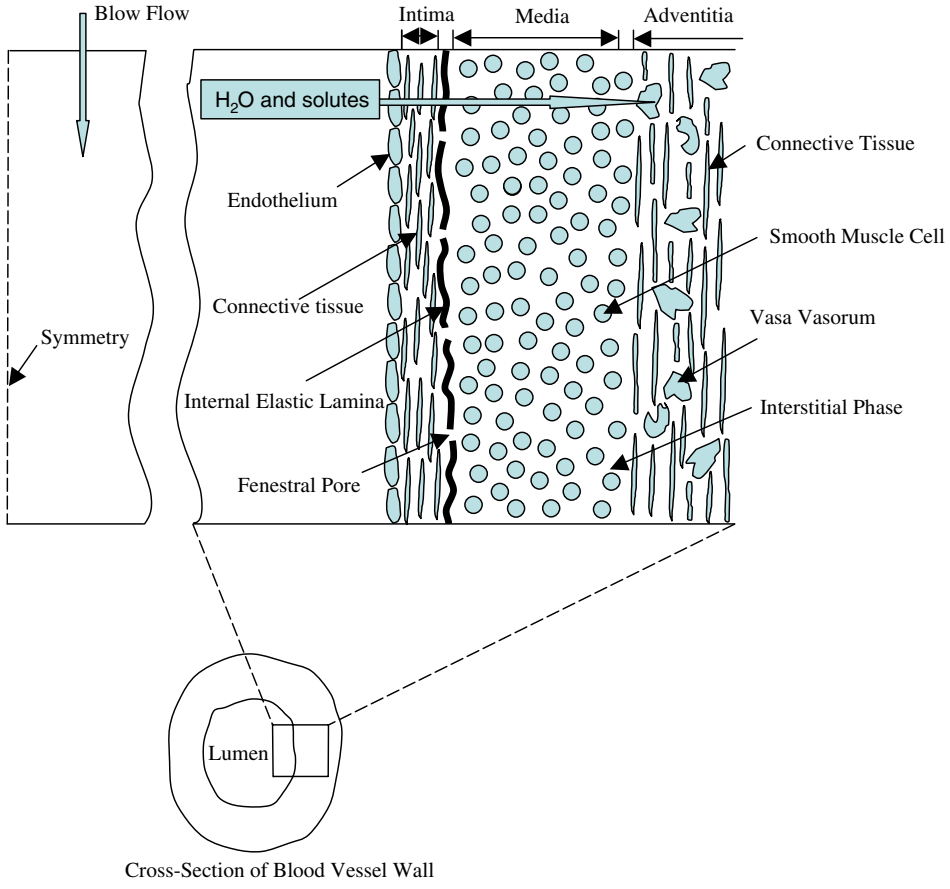

Fig. 1. Transverse sectional view of a blood vessel wall.

In the current study, a four-layer-wall model is presented which consists of the following five regions, lumen, endothelium, intima, IEL and media. The fundamental porous media equations are utilized to characterize the properties associated with the wall layers. Starting from these governing equations and the well established experimental data of the wall permeability and concentration profile in the media, the parameters associated with each layer are determined. Utilizing these parameters in our model, the effects of hypertension are studied. Since the intimal thickening is believed to be a very important factor in the process of atherogenesis, the model is then applied to a stenosed artery. The current model gives good estimation of velocity and species distributions in the blood lumen and within the artery wall.

2. Mathematical model

2.1. Lumen

In the arterial lumen, blood is treated as a homogeneous, isothermal and incompressible fluid. The blood flow can be described by the Navier–Stokes and continuity equations:

$$\frac{\partial \vec{u}_1}{\partial t} + (\vec{u}_1 \cdot \nabla)\vec{u}_1 - v_1 \nabla^2 \vec{u}_1 + \nabla p = 0 \tag{1}$$

$$\nabla \cdot \vec{u}_1 = 0 \tag{2}$$

where $\vec{u}_1$ is the velocity vector, p is the pressure and v is the apparent kinematic viscosity of the blood. It should be noted that the elaboration of non-Newtonian effects can be found in the work of Ai and Vafai [13].

In our study, the velocity field is computed in both the luminal and porous wall regions of an artery simultaneously. A generalized model is utilized to describe the filtration of plasma across the tissue layers constituting the wall [14–16]:

$$\frac{\rho}{\varepsilon}\left[\frac{\partial \vec{u}}{\partial t} + (\vec{u} \cdot \nabla)\vec{u}\right] = -\nabla p + \frac{\mu}{\varepsilon}\nabla^2 \vec{u} - \frac{\mu}{K_D}\vec{u} - \frac{\rho F \varepsilon}{K_D^{1/2}}[\vec{u} \cdot \vec{u}]J \tag{3}$$

In the luminal region, the species transport governing equation can be written as

$$\frac{\partial c_1}{\partial t} + \vec{u}_1 \nabla c_1 - D_1 \nabla^2 c_1 = 0 \tag{4}$$

where c_1 is the average species concentration associated with the fluid and D_1 is the diffusion coefficient. where $\vec{u}$

and $(\vec{u}\cdot\nabla)\vec{u}$ are the local volume-averaged quantities associated with the fluid, F is a function used in expressing inertia terms, ρ is the fluid density and K_D is the Darcy permeability. The quantities p and J are the average pressure inside the fluid and a unit vector oriented along the velocity vector $\vec{u}$, respectively. The generalized equation describing flow in a saturated porous medium allows satisfaction of no-slip boundary conditions. The generalized model gives the correct limiting behavior, reducing to Darcy's law in a uniform porous media and the Navier–Stokes equations in free fluid.

2.2. Endothelium and IEL

The endothelium and IEL are considered to be porous membranes in the current model, in which the volume flux is driven by both the hydraulic pressure and osmotic pressure. The governing equation for the fluid can be obtained from Eq. (3) as

$$\nabla p = -\frac{\mu_p}{K_D}\vec{u}_2 + \sigma_d R_g T \nabla c_2 + \tilde{\mu}_p \nabla^2 \vec{u}_2 \tag{5}$$

$$\nabla \cdot \vec{u}_2 = 0 \tag{6}$$

In the above equation, $\vec{u}_2$ is the velocity vector for the plasma, μ_p is the plasma viscosity, $\tilde{\mu}_p$ is the effective viscosity, K_D is the Darcy permeability and p is the pressure. The first term on the right-hand side of Eq. (3) represents the Darcy resistance for each wall layer while the second term describes the viscous force which is required to satisfy the no-slip boundary condition. For the last term, the effective viscosity $\tilde{\mu}_p$ is taken to be equal to μ_p in our study. Detailed models for $\tilde{\mu}_p$ can be found in Alazmi and Vafai [17]. The second term on the right-hand side of Eq. (5), accounts for the osmosis effects, where σ_d is the osmotic reflection coefficient, R_g is the universal gas constant and T is the absolute temperature.

The species transport is governed by the following equation:

$$\varepsilon\frac{\partial c_2}{\partial t} + \nabla\cdot(\gamma\vec{u}_2 c_2 - \tau\varepsilon D_2 \nabla c_2) = 0 \tag{7}$$

where c_2 is the species concentration in the fluid phase, ε the porosity, and τ is the tortuosity.

The term $\tau\varepsilon D_2$ is commonly considered to be the effective diffusion coefficient $D_{2,\text{eff}}$. It should be noted that the large molecules are reflected by the porous tissue layer which results in a reduced convective transport. This phenomenon is taken into account by adding a sieving coefficient γ in the convective term. The transport does not occur directly from point to point on the shortest distance inside the porous medium due to the solid matrix blockage. The tortuosity τ stands for the ratio of the straight line distance to the curved path length between the two points and it is assumed to be the same for all directions (isotropic). The tortuosity is usually determined experimentally [18,19].

2.3. Intima and media

The intima and media are also modeled as homogeneous porous media. Since the average spacing between fibers is significant relative to the wall thickness, the fiber-induced velocity boundary layers should be included. Due to physiological range of parameters, Eq. (3) can be simplified as [15]

$$\nabla p = -\frac{\mu_p}{K_D}\vec{u}_3 + \tilde{\mu}_p \nabla^2 \vec{u}_3 \tag{8}$$

The continuity equation is given as

$$\nabla \cdot \vec{u}_3 = 0 \tag{9}$$

In the porous wall region, neglecting the dispersion and fluid–solid interaction terms, the species transport process can be described by the following volume-averaged advection–diffusion equation [15,19,20]:

$$\varepsilon\frac{\partial c_3}{\partial t} + \nabla\cdot(\gamma\vec{u}_3 c_3 - \tau\varepsilon D_3 \nabla c_3) + \varepsilon k c_3 = 0 \tag{10}$$

The LDL reaction rate on the surface of SMC is approximated by a first-order reaction. The reaction is considered only in the media layer, which means that the effective first-order reaction rate coefficient k equals to zero in the other wall layers.

2.4. Geometry and boundary conditions

The artery is modeled as a straight tube with the luminal radius of $R_0 = 0.31$ cm and length of $L_{un} = 36R_0 = 11.16$ cm. A fully developed (parabolic) velocity profile with the mean velocity $U_0 = 16.9$ cm/s is specified at the inlet. The specified physiological and geometrical dimensions are based on typical values found in the literatures for the arteries. The density and apparent viscosity of blood are $\rho = 1.05$ g/cm^3 and $\mu = 0.035$ g/(cm s), which lead to a Reynolds number of $Re = 316$. The diffusivity of LDL in the blood is 5×10^{-8} cm^2/s. The thickness of each wall layer is listed in Table 1 [10,12], which results in a total thickness of wall layer of $L_w = 0.0214$ cm $= 0.069R_0$.

The following physiologically consistent boundary conditions for fluid and species are specified, as shown in Fig. 2.

2.5. Boundary conditions for fluid

A fully develop (parabolic) velocity profile at the inlet of the arterial lumen

Table 1
Thickness of the considered wall layers

Wall layer	Thickness (μm)
Endothelium	2.0
Intima	10.0
IEL	2.0
Media	200.0

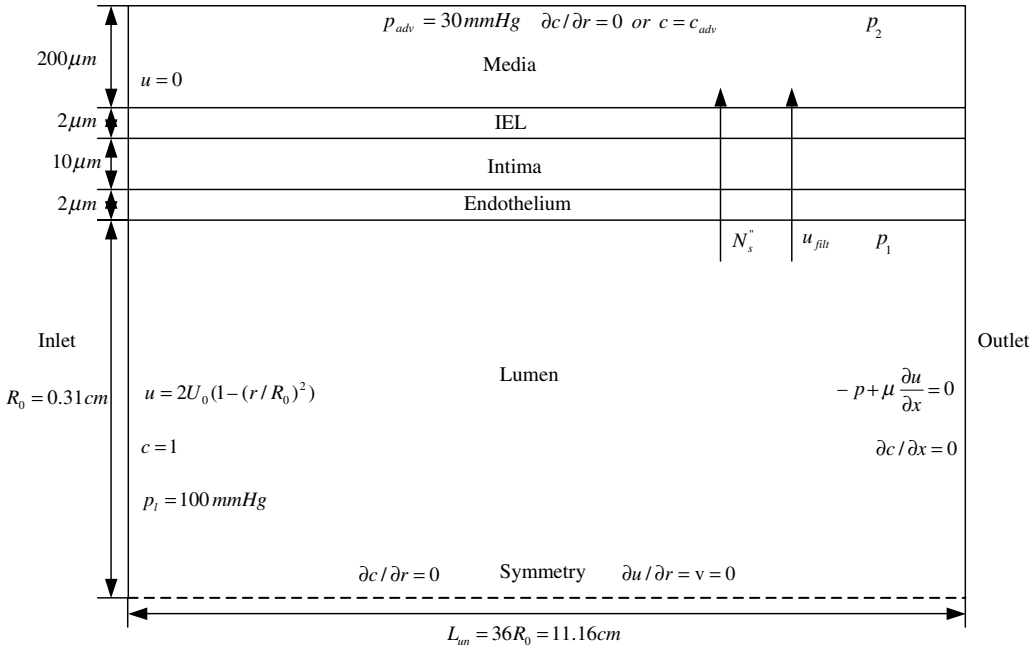

Fig. 2. The geometry and boundary conditions.

$$u = 2U_0(1-(r/R_0)^2) \quad \text{and} \quad v = 0 \quad \text{for } 0 \leqslant r \leqslant R_0, \ x = 0 \tag{11}$$

Zero axial velocity at the corresponding inlet of each wall layer

$$u = 0 \quad \text{for } R_0 \leqslant r \leqslant 1.069R_0, \ x = 0 \tag{12}$$

A traction-free condition at the outlet of the lumen and each wall layer

$$-p + \mu\frac{\partial u}{\partial x} = 0 \quad \text{for } 0 \leqslant r \leqslant 1.069R_0, \ x = 36R_0 \tag{13}$$

Zero transverse velocity gradient and zero cross flow on the axis of symmetry

$$\partial u/\partial r = v = 0 \quad \text{on } r = 0 \tag{14}$$

The near-wall normal velocity component is equal to the transmural filtration velocity

$$u_1 = u_2 = u_3 = u_{\text{filt}} \tag{15}$$

where u_{filt} is the filtration velocity through the wall.

Constant pressure at the inlet and at the adventitial vasa vasorum

$$p_{\text{l}} = 100 \text{ mm Hg} \quad \text{for } 0 \leqslant r \leqslant R_0, \ x = 0 \tag{16}$$

$$p_{\text{adv}} = 30 \text{ mm Hg} \quad \text{for } r = 1.069R_0 \tag{17}$$

2.6. Boundary conditions for species

Constant LDL inlet concentration

$$c = C/C_0 = 1 \quad \text{for } 0 \leqslant r \leqslant R_0, \ x = 0 \tag{18}$$

where c is the nondimensionalized concentration and C_0 is the reference concentration. C_0 is taken to be $C_0 =$ 1.2 mg/ml which fits data in the range of LDL concentrations $C_0 = 0.5$–2 mg/ml for human blood.

Zero transverse concentration gradient on the axis of symmetry

$$\partial c/\partial r = 0 \quad \text{on } r = 0 \tag{19}$$

Zero axial concentration gradient at the outlet of the lumen and for each wall layer

$$\partial c/\partial x = 0 \quad \text{for } 0 \leqslant r \leqslant 1.069R_0, \ x = 36R_0 \tag{20}$$

Boundary conditions for the concentration at the interfaces of lumen and the arterial walls can be written as

$$(-D_1\nabla c_1 + u_1 c_1)\cdot n_1 = (-\tau\varepsilon D_2\nabla c_2 + \gamma u_2 c_2)\cdot n_2 = N_{\text{s}}'' \tag{21}$$

where N_{s}'' and n are the mass flux of solute per unit area through the wall and the unit vector normal to the interface, respectively.

3. Simulations

The transport processes in the lumen, intima and media are coupled by the flux across the endothelium and IEL which is traditionally modeled using the Kedem–Katchalsky equations [7,10]. A detailed description of the pore theory and the theoretical characterization of its coefficients can be found in Kedem and Katchalsky [21], Curry [22], Deen [23], Jo et al. [24], Wang and Tarbell [25], and Michel and Curry [26]. However, complex computations are involved to theoretically estimate the coefficients using the pore theory. The equations here are solved using the Galerkin finite element method. Detailed solution

algorithm and method used in the current work are given in the Ref. [27].

Instead of using the pore theory to model the endothelium and the internal elastic lamina (IEL), we will utilize a simplified porous media theory to model these two layers. This simplified mathematical model allows us to define the relationship between the set of physical parameters characterizing each wall layer. Therefore, incorporating experimentally determined data, we can directly estimate these coefficients.

We start with the filtration velocity, u_{filt}, and the mass flux, N_s'', whose values have been determined experimentally. We introduce the definition of the effective permeability. The filtration velocity u_{filt} is given in terms of its driving force, $-\Delta p = p_1 - p_2$ and the effective permeability $K_{\text{D,eff}}$

$$u_{\text{filt}} = -\frac{K_{\text{D,eff}}}{\mu_p L}\Delta p \tag{22}$$

where L is the thickness of the wall, and p_1 and p_2 are the pressure on each side of the layer. The relationship between $K_{\text{D,eff}}$ and K_{D} can be obtained by solving Eq. (5) satisfying the no-slip boundary conditions at the top and bottom boundaries [28].

$$K_{\text{D,eff}} = K_{\text{D}}[1 - \tanh(L/(2\sqrt{K_{\text{D}}}))/(L/(2\sqrt{K_{\text{D}}}))] \tag{23}$$

The average concentration within a wall layer is defined as $c_{\text{avg}} = w_1 c_1 + w_2 c_2$, where w_1 and w_2 are suitable weighting functions independent of the concentration and c_1 and c_2 are lower and upper concentration for each of the layers. These weighting functions can be calculated assuming that the concentration inside the layer varies only along the normal direction. Under the steady state conditions, the governing equation for the concentration field Eq. (10) reduces to

$$-D_{\text{eff}} c''(x) + \gamma u \cdot n c'(x) + \varepsilon k c(x) = 0, \quad x \in (0, L) \tag{24}$$

$$c(0) = c_1 \tag{25a}$$

$$c(L) = c_2 \tag{25b}$$

where L is the thickness of the layer.

It should be noted that the first-order reaction coefficient k is taken as zero in the endothelium, intima and IEL. The exact solution for this boundary value problem is given as

$$c(x) = ((c_1 e^{\lambda_2 L} - c_2)e^{\lambda_1 x} - (c_1 e^{\lambda_1 L} - c_2)e^{\lambda_2 x})/(e^{\lambda_2 L} - e^{\lambda_1 L}) \tag{26}$$

By integrating $c(x)$ over $(0, L)$, we can obtain the average concentration, which can be used to define analytical expressions for the weighting functions w_1 and w_2 with respect to the arguments D_{eff}, γ, $u \cdot n$, k

$$c_{\text{avg}} = \frac{\int_0^L c(x)\mathrm{d}x}{L} = w_1 c_1 + w_2 c_2 \tag{27}$$

where the eigenvalues $\lambda_{1,2}$ are given as

$$\lambda_{1,2} = \frac{\gamma u \cdot n \pm \sqrt{(\gamma u \cdot n)^2 + 4D_{\text{eff}}\varepsilon k}}{2D_{\text{eff}}} \tag{28}$$

$$w_1 = \frac{(\lambda_2 - \lambda_1)e^{(\lambda_1+\lambda_2)L} - \lambda_2 e^{\lambda_2 L} + \lambda_1 e^{\lambda_1 L}}{\lambda_1\lambda_2(e^{\lambda_2 L} - e^{\lambda_1 L})} \quad \text{and}$$
$$w_2 = \frac{\lambda_1 e^{\lambda_2 L} - \lambda_2 e^{\lambda_1 L} + \lambda_2 - \lambda_1}{\lambda_1\lambda_2(e^{\lambda_2 L} - e^{\lambda_1 L})} \tag{29}$$

In the work of Prosi et al. [10], the resistances associated with the diffusion and convection processes are approximated as $R_{\text{diff}} = -L/D_{\text{eff}}$ and $R_{\text{conv}} = (c_1 - c_2)/\gamma u \cdot n c_{\text{avg}}$ respectively. This approximation for the diffusion resistance can only be made when the concentration gradient can be assumed linearly dependent on the boundary concentration. From Eq. (24), it is clear that this only happens when the second term and third term are relatively small, which indicates that the reaction inside the layer is small and that the convection is negligible. For the media, this approximation is not valid due to the convection-dominant transport mode and the large reaction coefficient. It should be noted that utilizing a linear approximation to estimate the concentration gradient and the average concentration in the media, which is effectively what has been done in Prosi et al. [10], leads to substantial errors. In our model, rather than approximating the concentration gradient and the average concentration, we utilize the analytical solutions to ensure the continuity of the specified species fluxes across the interfaces.

Another boundary condition at the media–adventitia interface $\partial c_{\text{adv}}/\partial n = 0$ is also incorporated in our model. As such we will develop a revised solution for Eq. (24) using the following boundary conditions:

$$c(0) = c_{\text{med}}^+ \tag{30a}$$

$$\frac{\partial c(L_{\text{med}})}{\partial n} = 0 \tag{30b}$$

where L_{med} is the thickness of the media layer and c_{med}^+ is the specified concentration at media–adventitia interface, we obtain the concentration distribution as

$$c(x) = \frac{c_{\text{med}}^+(\lambda_1 e^{\lambda_1 L_{\text{med}}} e^{\lambda_2 x} - \lambda_2 e^{\lambda_2 L_{\text{med}}} e^{\lambda_1 x})}{\lambda_1 e^{\lambda_1 L_{\text{med}}} - \lambda_2 e^{\lambda_2 L_{\text{med}}}} \tag{31}$$

where $\lambda_{1,2}$ have the same forms as those given in Eq. (28).

Hence the average concentration for the new distribution given in Eq. (31) is found to be

$$c_{\text{avg,med}} = \frac{c_{\text{med}}^+[(\lambda_1^2 - \lambda_2^2)e^{(\lambda_1+\lambda_2)L_{\text{med}}} - \lambda_2^2 e^{\lambda_1 L_{\text{med}}} + \lambda_1^2 e^{\lambda_2 L_{\text{med}}})]}{\lambda_1\lambda_2(\lambda_1 e^{\lambda_1 L_{\text{med}}} - \lambda_2 e^{\lambda_2 L_{\text{med}}})L_{\text{med}}} \tag{32}$$

The concentration gradient at the left boundary is found to be

$$\frac{\partial c(0)}{\partial n} = \nabla c_{\text{med}}^+ = \frac{c_{\text{med}}^+ \lambda_1\lambda_2(e^{\lambda_1 L_{\text{med}}} - e^{\lambda_2 L_{\text{med}}})}{\lambda_1 e^{\lambda_1 L_{\text{med}}} - \lambda_2 e^{\lambda_2 L_{\text{med}}}} \tag{33}$$

4. Determination of the parameters

A multilayer model is utilized, which accounts for a relatively detailed structure of the wall. Its components include the lumen, the lumen–endothelium interface, endothelium, endothelium–intima interface, intima, intima–IEL interface, IEL, IEL–media interface, and media (which is the thickest part of the arterial wall).

Mass transfer through the arterial wall has been studied by Jo et al. [24], Wang and Tarbell [25], Tarbell et al. [29], Huang et al. [30], Huang et al. [31], Huang et al. [32] and Truskey et al. [33]. The current model is based on experimental data that involve both the filtration of plasma through the artery wall and the transport process of chemicals. The primary sources of data come from the experimental work of Meyer et al. [34] where filtration velocities and LDL concentration profiles are measured at the same time for rabbit aortas and the analysis of Yuan et al. [35] where the Peclet numbers in the wall layers are either estimated using the fiber matrix model or obtained through experimental measurements.

4.1. Model for filtration

The parameters characterizing the filtration of plasma into the wall can be determined employing a circuit analogy. The viscosity of the plasma μ_p is taken as $\mu_p = 0.72 \times 10^{-2}$ g/(cm s). In the literature, there is a good agreement on the order of magnitude of the media's Darcy permeability, 10^{-14}, which has been experimentally evaluated by Whale et al. [36]. On the other hand, the order of magnitude of $K_{D,int}$ (the Darcy permeability associated with the intima) is 10^{-12} cm^2, which is hundred fold greater than the measured value for the media's permeability, 10^{-14} cm^2 [31].

The values of permeability of the intima and media are in general well established [8,10,31,32]. Based on these works, we set the value of permeability of media as $K_{D,med} = 2.0 \times 10^{-14}$ cm^2 and the value of permeability of intima as $K_{D,int} = 2.2 \times 10^{-12}$ cm^2.

Neglecting the flux due to osmosis, the electrical analogy for the plasma filtration features four resistances in series, corresponding to endothelium, intima, IEL, and media, respectively. By applying the electric analogy, we obtain

$$R_{tot} = \frac{p_1 - p_2}{u_{filt}} = \frac{\mu_{end} L_{end}}{K_{D_{eff,end}}} + \frac{\mu_{int} L_{int}}{K_{D_{eff,int}}} + \frac{\mu_{iel} L_{iel}}{K_{D_{eff,iel}}} + \frac{\mu_{med} L_{med}}{K_{D_{eff,med}}} \tag{34}$$

With the transmural pressure jump $p_1 - p_2 = 70$ mm Hg and $u_{filt} = 1.78 \times 10^{-6}$ cm/s as reported in Meyer et al. [34], which are coherent with the measurements presented in Tarbell et al. [37], Dull et al. [38], Huang et al. [32], Deng et al. [39], Tedgui and Lever [40], we obtain the total resistance of $R_{tot} = 5.24135 \times 10^{10}$ g/cm^2 s.

The porosities are 5×10^{-4}, 0.96, 4×10^{-3} and 0.15 for endothelium, intima, IEL and media, respectively [8,10,

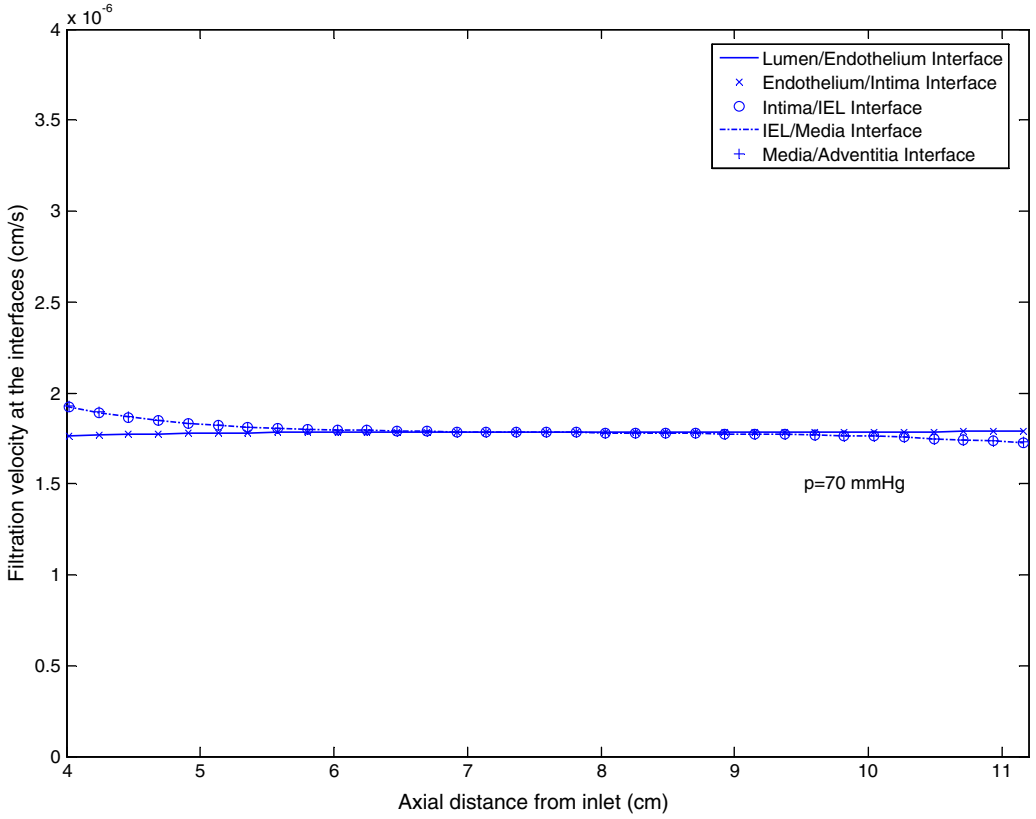

Fig. 3. Calculated filtration velocities at the interfaces.

35,41]. Based on Eq. (23), we can calculate the effective permeabilities for the intima and media. The calculated permeability for the intima and media are $K_{D_{eff,int}} = 2.19347 \times 10^{-12}$ cm^2 and $K_{D_{eff,med}} = 1.99997 \times 10^{-14}$ cm^2, which trans-

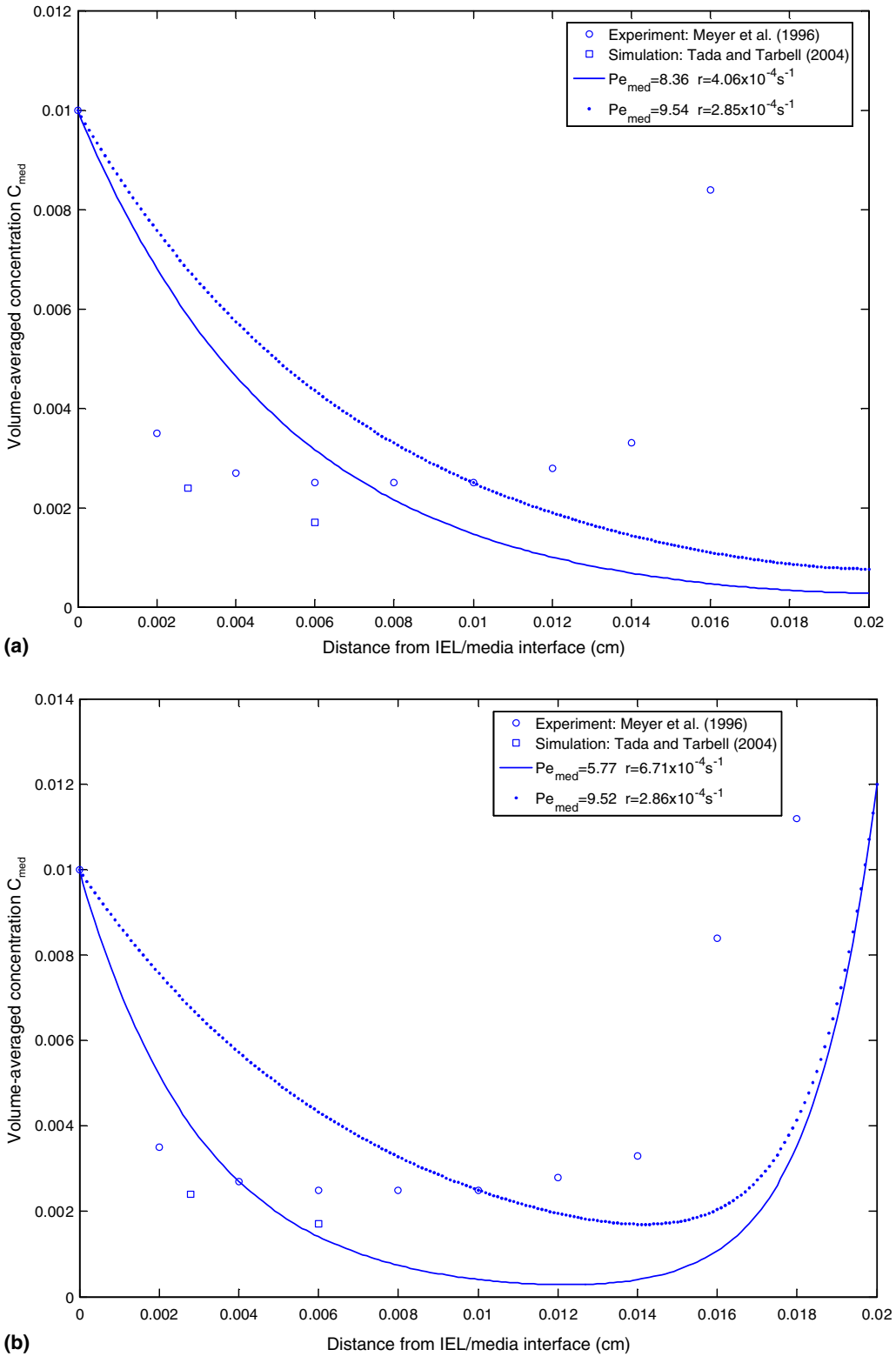

Fig. 4. (a) Calculated volume-averaged LDL concentration profile in the media at transmural pressure of 70 mm Hg (gradient-free concentration boundary condition). (b) Calculated volume-averaged LDL concentration profile in the media at transmural pressure of 70 mm Hg with specified boundary concentration at the media/adventitia interface $\bar{c}_{adv} = 1.2 \times 10^{-2}$.

lates into the following resistances of $R_{int} = 3.28 \times 10^6$ g/cm^2 s and $R_{med} = 7.2 \times 10^9$ g/cm^2 s, for intima and media respectively.

The resistance for the endothelium layer is about one hundred times greater than the one for IEL

$$R_{end} + R_{iel} = 1.01R_{end} = R_{tot} - R_{int} - R_{med} = 4.521 \times 10^{10} \text{ g/cm}^2 \text{ s} \quad (35)$$

This results in $R_{end} = 4.476 \times 10^{10}$ g/cm^2 s and $R_{iel} = 4.476 \times 10^8$ g/cm^2 s which agrees well with the values obtained by Karner et al. [7] based on pore theory.

As such, we obtain $K_{D_{eff,end}} = 3.21697 \times 10^{-17}$ cm^2 and $K_{D_{eff,iel}} = 3.21697 \times 10^{-15}$ cm^2. Hence the Darcy permeability associated with the endothelium and IEL can be calculated from Eq. (23) using an iterative method $K_{D,end} = 3.21715 \times 10^{-17}$ cm^2 and $K_{D,iel} = 3.21880 \times 10^{-14}$ cm^2. As shown in Fig. 3, we can see that the calculated radial velocity across each interface corresponds well with the specified filtration velocity of $u_{filt} = 1.78 \times 10^{-6}$ cm/s.

4.2. Model for species transport

An electrical analog is utilized in the model used by Prosi et al. [10], in which the media is divided into two equal parts to take into account the degradation of solute due to chemical reactions. However, it should be noted that special attention needs to be given to the media layer due to the large concentration gradient at the IEL/media interface.

We start by specifying the parameter values that are experimentally determined. As such, the porosity of the media is set to $\varepsilon_{med} = 0.15$ and the effective diffusivity of LDL is taken as $D_{eff,med} = 5.0 \times 10^{-10}$ cm^2/s, based on the data reported in the work of Truskey et al. [42], Truskey et al. [33], Karner et al. [7], Stangeby and Ethier [8] and references therein. With these values, we will estimate the concentration profile inside the different layers. Details of the LDL mass transport simulation and the effects of hypertension on an artery were analyzed in Yang and Vafai [43]. The results in Yang and Vafai [43] constitute a robust framework for analyzing the LDL transport in an artery.

The volume-averaged LDL concentration in the media is about 2.5×10^{-3} under the transmural pressure of 70 mm Hg based on the data reported in Meyer et al. [34]. Considering the polarization effect at the interface between the lumen and the wall, the concentration at the interface is taken to be $c_l = 1.0262$ [10]. It should be noted that the value of the polarization effect strongly depends on the filtration velocity which has been studied by Wada and Karino [11]. The following sequence of steps will describe the methodology for estimating the unknown parameters characterizing different layers.

4.3. Determination of the overall mass flux crossing the arterial wall

The flux of LDL into the arterial wall depends on the plasma concentration and the apparent permeability, which is similar for the aorta of humans, monkeys, rabbits, and pigeons [44]. Based on the works of Truskey et al. [33] and Huang and Tarbell [45], we assign the value of the apparent permeability of artery wall as $P_{tot} = 2 \times 10^{-8}$ cm/s.

According to the definition of P_{tot}, the overall mass flux can be given as

$$N_s'' = P_{tot} c_l = 2.0524 \times 10^{-8} \text{ cm/s} \quad (36)$$

which should be a constant throughout the wall layers. At the lumen/endothelium interface, we obtain from Eq. (21)

$$N_s'' = -D_{eff,end} \nabla c_l + \gamma_{end} u_{filt} c_l \quad (37)$$

where c_l is the concentration at the endothelium/intima interface.

We define the Peclet number associated with the endothelium Pe_{end} as

$$Pe_{end} = \gamma_{end} u_{filt} / (D_{eff,end}/L_{end}) \quad (38)$$

It is stated in Yuan et al. [35] that the convection is the dominant mode of transport ($Pe_{end} \sim 10$) when the transmural pressure is greater than 70 mm Hg. As such, we set $Pe_{end} = 5$ and rewrite Eq. (37) in terms of Pe_{end} as

$$P_{tot} c_l = -D_{eff,end} \nabla c_l + (Pe_{end} D_{eff,end}/L_{end}) c_l \quad (39)$$

The expression for ∇c_l in terms of Pe_{end} can be acquired from Eq. (26) with the reaction coefficient of $k = 0$

$$\nabla c_l = \frac{Pe_{end}(c_{int}^+ - c_l)}{L_{end}(e^{Pe_{end}} - 1)} \quad (40)$$

By dividing c_l on both sides of Eq. (39) and neglecting the small term c_{int}^+/c_l, we obtain

Table 2
Values of the constants and parameters in each region

	Fluid	Endothelium	Intima	IEL	Media
Viscosity (g/cm^2 s)	0.035	0.0072	0.0072	0.0072	0.0072
Porosity		0.0005	0.96	0.004	0.15
Diffusivity (cm^2/s)	2.867×10^{-7}	8.154×10^{-13}	5.0×10^{-8}	3.18×10^{-11}	5.0×10^{-10}
Permeability (cm^2)		3.21715×10^{-17}	2.2×10^{-12}	3.2188×10^{-15}	2.0×10^{-14}
Sieving coefficient		1.145×10^{-2}	1.7084×10^{-1}	1.7048×10^{-1}	1.34×10^{-1}
Reaction coefficient (s^{-1})					2.85×10^{-4}

$$P_{\text{tot}} = \frac{D_{\text{eff,end}} Pe_{\text{end}} e^{Pe_{\text{end}}}}{L_{\text{end}}(e^{Pe_{\text{end}}} - 1)} \tag{41}$$

When $Pe_{\text{end}} = 5$, we obtain $D_{\text{eff,end}} = 8.154 \times 10^{-13}$ cm^2/s and $\gamma_{\text{end}} = 1.145 \times 10^{-2}$.

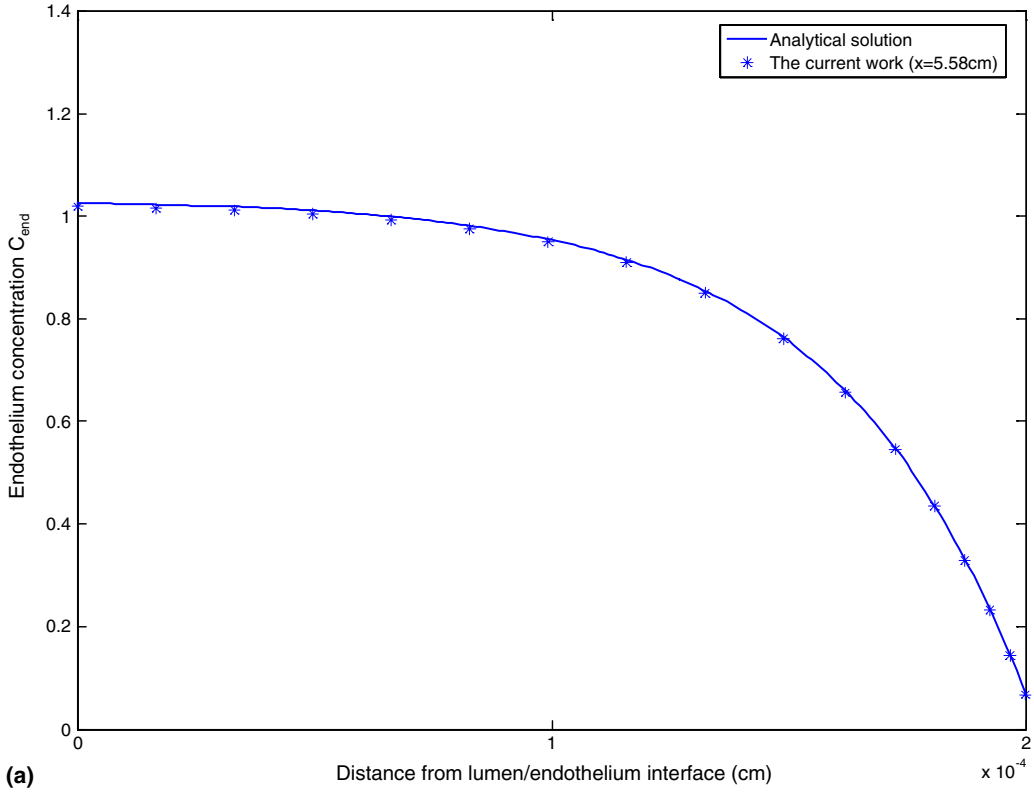

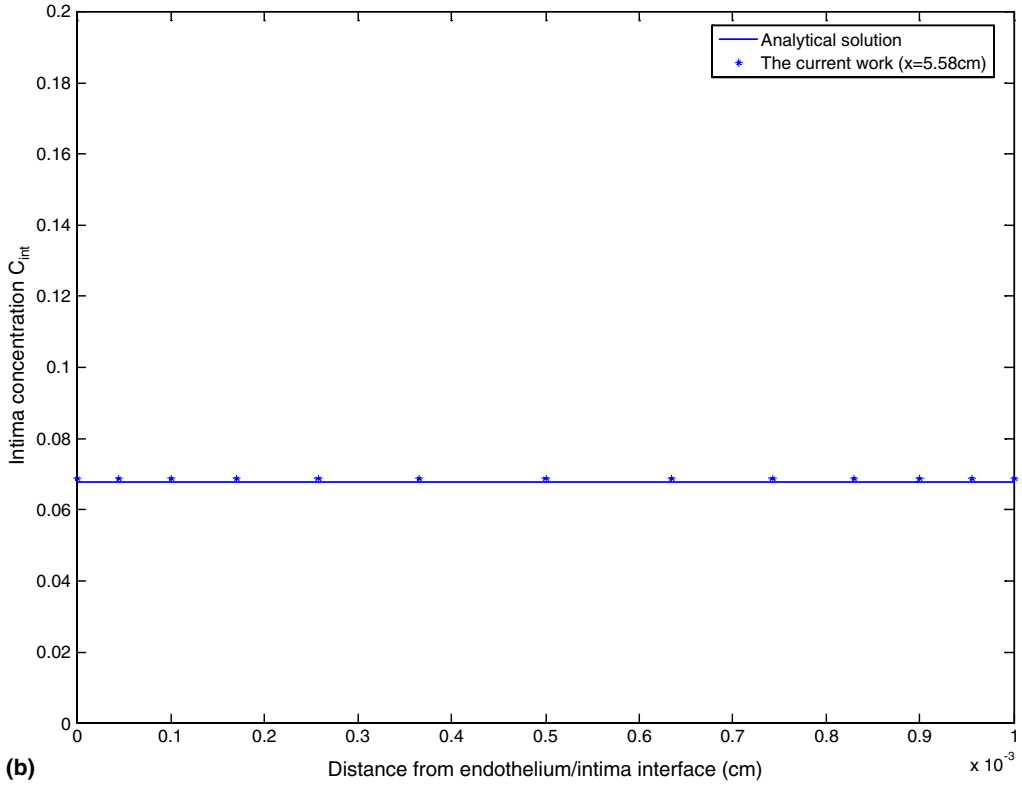

Fig. 5. (a) Comparison between the numerical results and the analytical solution for concentration profile in the endothelium. (b) Comparison between the numerical results and the analytical solution for concentration profile in the intima.

4.4. Determination of Pe_{med} and k

The diffusivity in the intima is about hundred fold greater than that which is in the media, according to the work of Huang et al. [31]. Therefore, the diffusivity in the intima is taken as $D_{\text{eff,int}} = 100 \times D_{\text{eff,med}} = 5.0 \times 10^{-8}$ cm^2/s.

The chemical reaction and the corresponding consumption of solute are due to its uptake by the smooth muscle

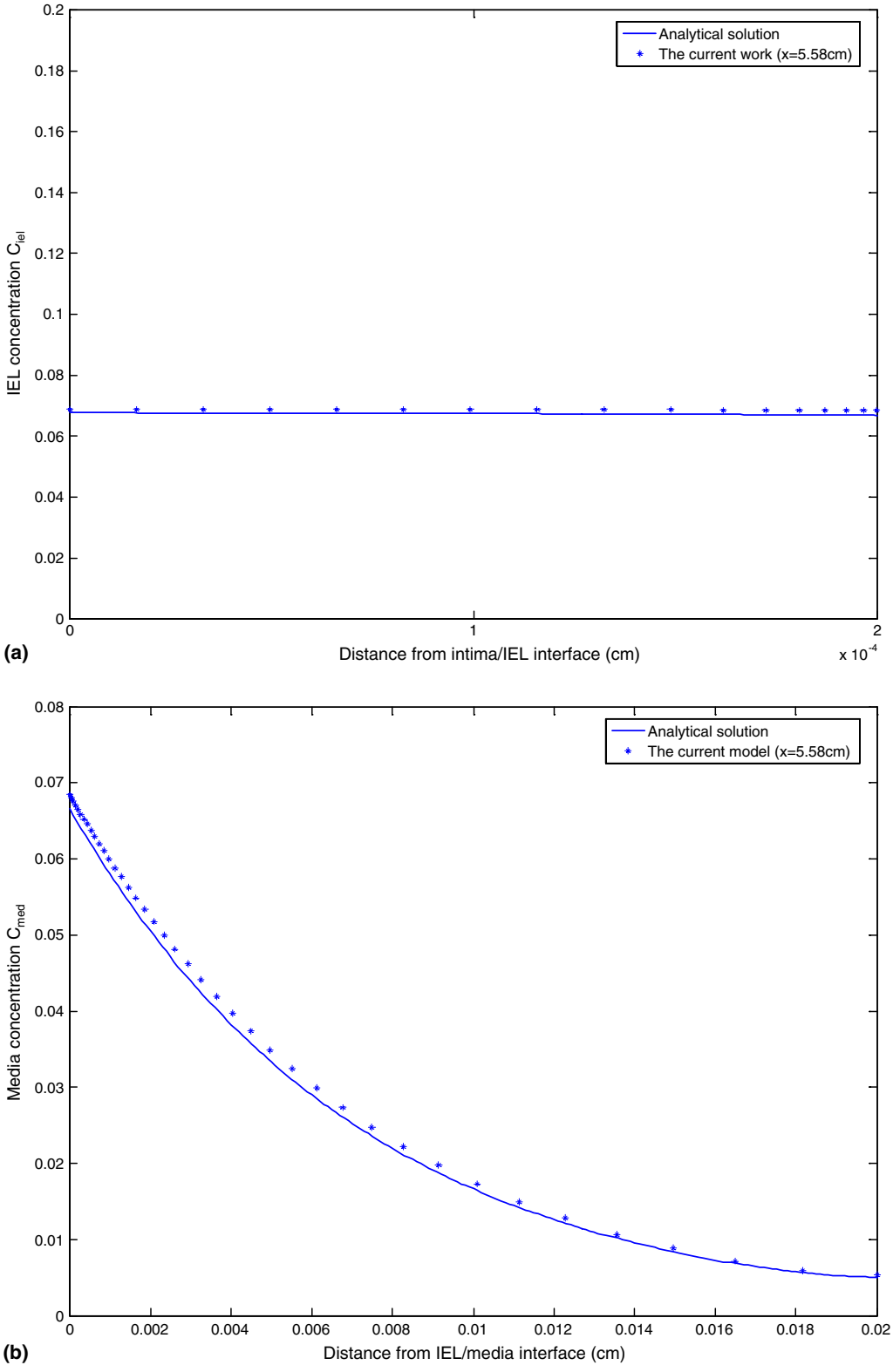

Fig. 6. (a) Comparison between the numerical results and the analytical solution for concentration profile in the IEL. (b) Comparison between the numerical results and the analytical solution for concentration profile in the media.

cells (SMCs). SMCs are considered to have a reactive surface but are impermeable to water flux due to the relatively low hydraulic conductance of the cell membrane. Since SMCs are assumed to distribute uniformly in the media,

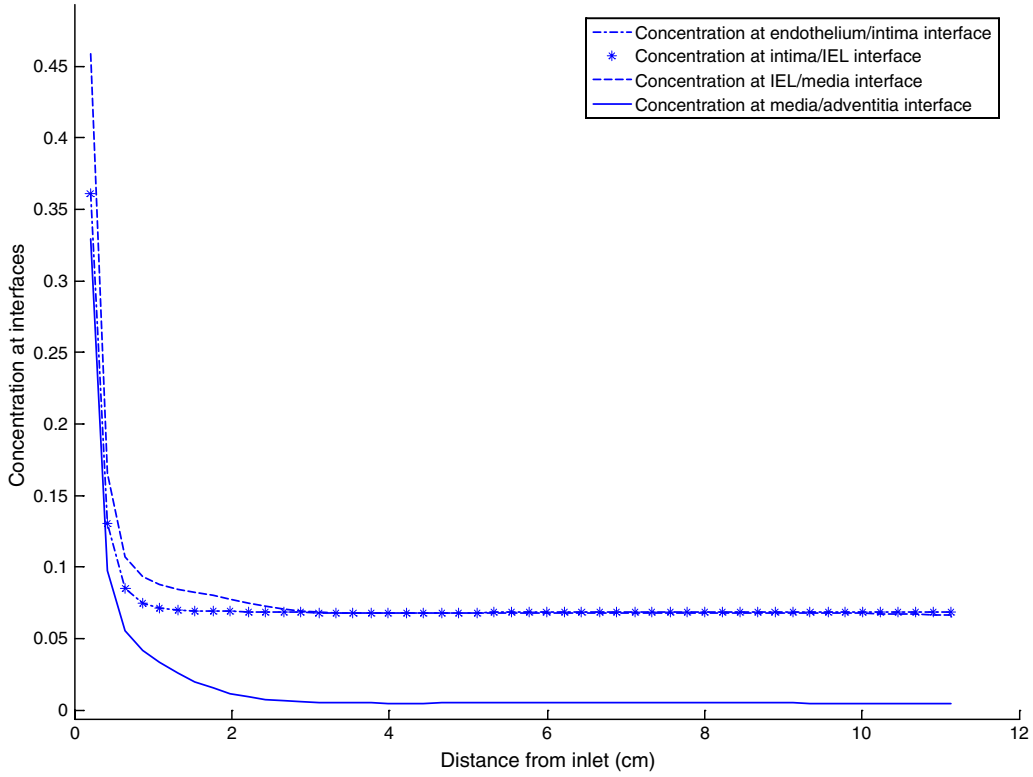

Fig. 7. Concentration profiles at the endothelium/intima, intima/IEL, IEL/media and media/adventitia interfaces.

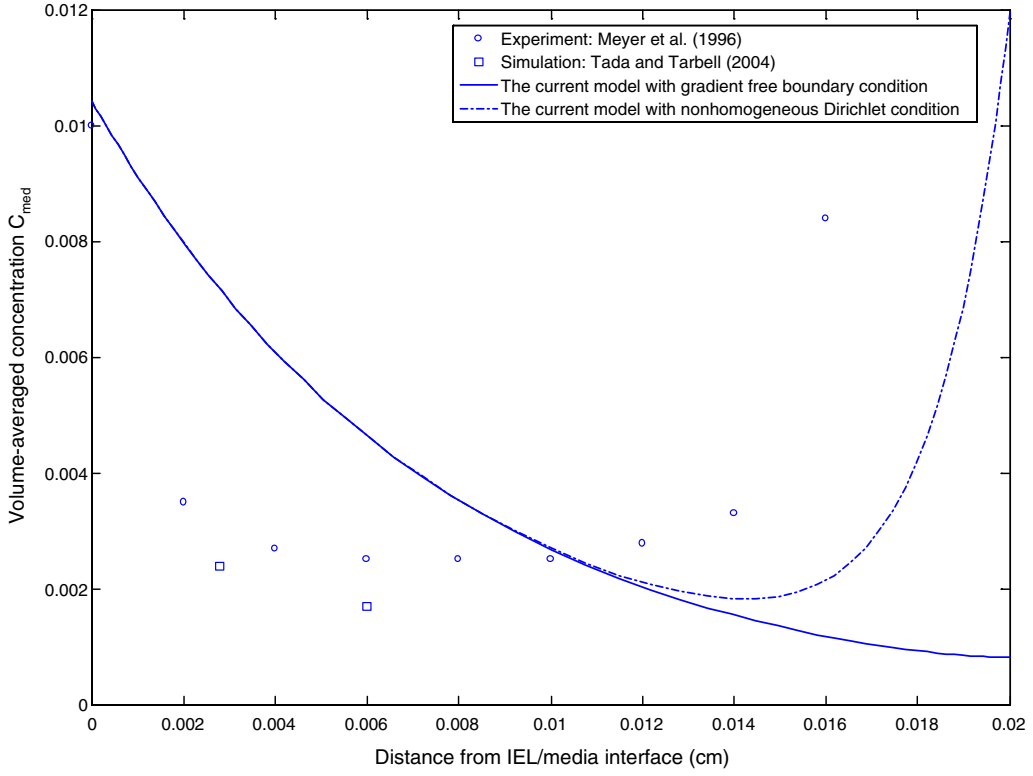

Fig. 8. Concentration profiles in the media using different boundary conditions at media/adventitia interface.

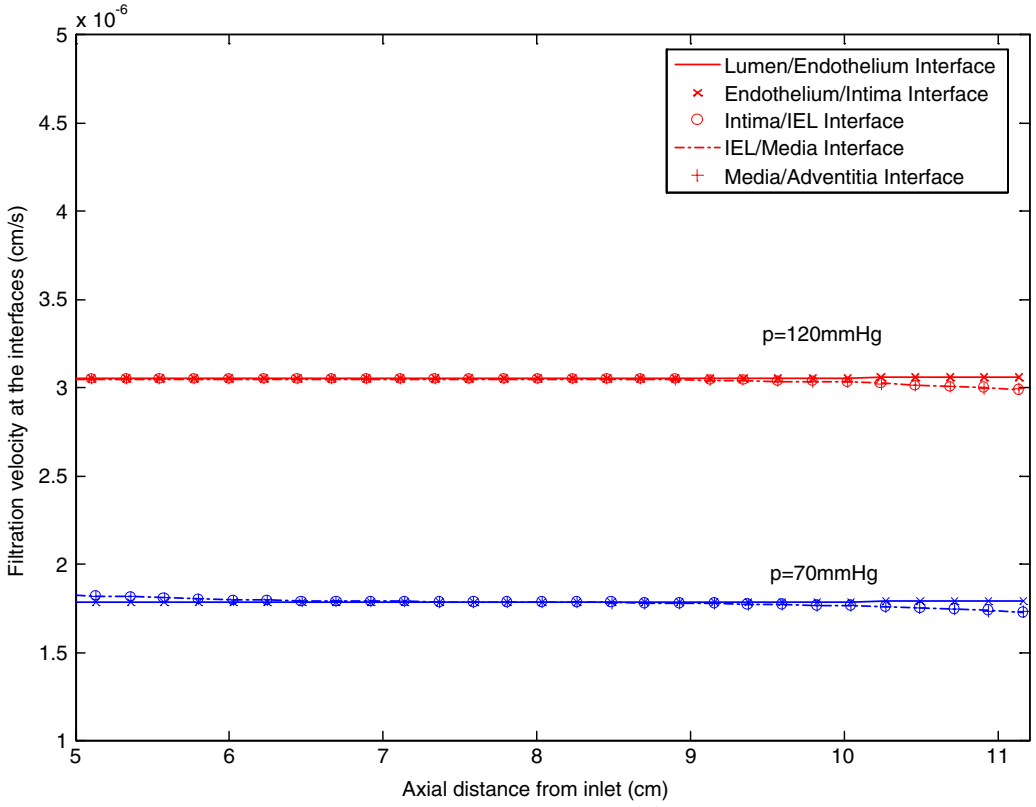

Fig. 9. Filtration velocity comparison under different transmural pressures.

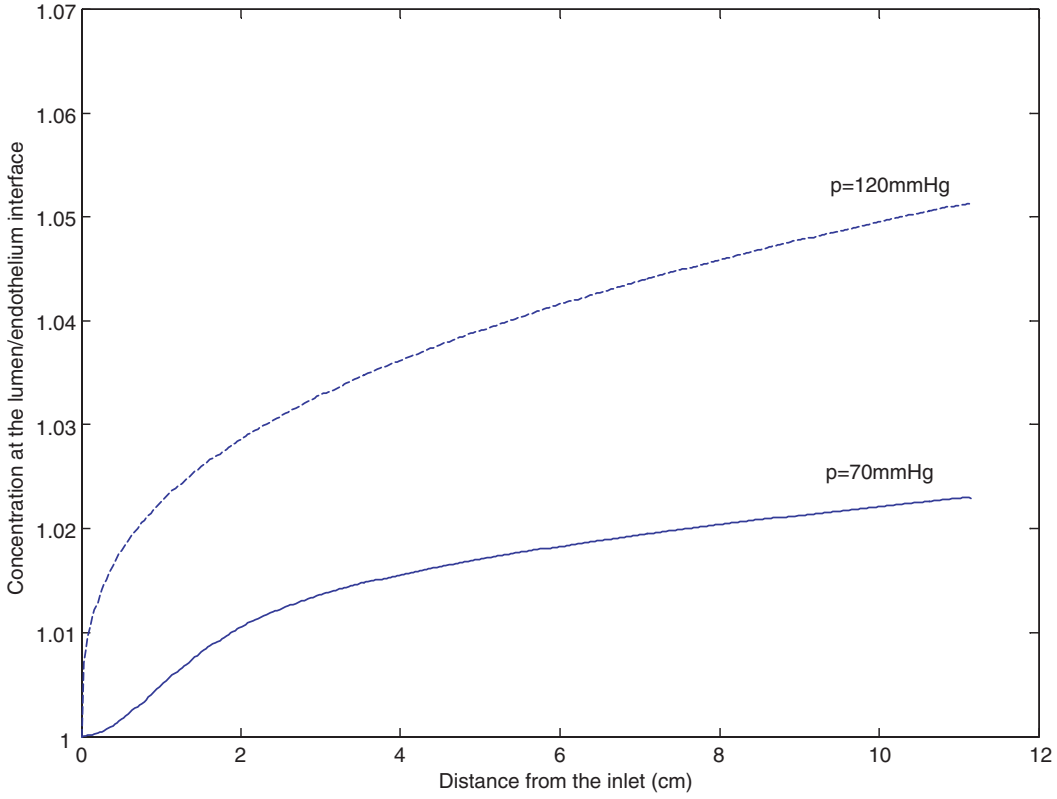

Fig. 10. Concentration profile at the lumen/endothelium interface.

the chemical reaction is homogeneously distributed in space that takes place across the entire width of the layer.

From the experimental results of Meyer et al. [34], we specify the concentration at the IEL/media interface to be $c^{+}_{\mathrm{med}} = \bar{c}^{+}_{\mathrm{med}}/\varepsilon_{\mathrm{med}} = 6.6667 \times 10^{-2}$, where $\bar{c}^{+}_{\mathrm{med}}$ is the volume-averaged concentration in the media. We define the Peclet number in the media as

$$Pe_{\mathrm{med}} = \gamma_{\mathrm{med}} u_{\mathrm{filt}} / (D_{\mathrm{eff,med}}/L_{\mathrm{med}}) \tag{42}$$

In terms of Pe_{med}, Eq. (24) can be rewritten as

$$c''(x) - Pe_{\mathrm{med}} c'(x)/L_{\mathrm{med}} - \varepsilon_{\mathrm{med}} k c(x)/D_{\mathrm{eff,med}} = 0 \tag{43}$$

and $\lambda_{1,2}$ can be rewritten as

$$\lambda_{1,2} = \frac{Pe_{\mathrm{med}}}{2L_{\mathrm{med}}} \pm \sqrt{\left(\frac{Pe_{\mathrm{med}}}{2L_{\mathrm{med}}}\right)^2 + \frac{\varepsilon_{\mathrm{med}} k}{D_{\mathrm{eff,med}}}} \tag{44}$$

When the gradient-free concentration boundary condition is applied, the mean concentration $c_{\mathrm{avg,med}}$ has the same expression as that given by Eq. (32) and the expression for the concentration in the middle of media can be obtained as

$$c(L_{\mathrm{med}}/2) = \frac{c^{+}_{\mathrm{med}}\left(\lambda_1 e^{\lambda_1 L_{\mathrm{med}}} e^{\lambda_2 (L_{\mathrm{med}}/2)} - \lambda_2 e^{\lambda_2 L_{\mathrm{med}}} e^{\lambda_1 (L_{\mathrm{med}}/2)}\right)}{\lambda_1 e^{\lambda_1 L_{\mathrm{med}}} - \lambda_2 e^{\lambda_2 L_{\mathrm{med}}}} \tag{45}$$

The mass flux across the in the IEL/media interface is given by

$$N''_{\mathrm{s}} = -D_{\mathrm{eff,med}} \nabla c^{+}_{\mathrm{med}} + \gamma_{\mathrm{med}} u \cdot n c^{+}_{\mathrm{med}} \tag{46}$$

By letting either the mean concentration $\bar{c}_{\mathrm{avg,med}}$ or the concentration in the middle of media $\bar{c}(L_{\mathrm{med}}/2)$ to be equal to the measured value of 2.5×10^{-3} and combining it with Eq. (46), we will have a nonlinear system of two equations for two unknowns k and Pe_{med}, respectively. We can solve these two sets of equations using an iterative method. This results in

$$Pe_{\mathrm{med}} = 8.36 \quad \text{and} \quad r = 4.06 \times 10^{-4}\ \mathrm{s}^{-1}$$
$$\text{for the case } \bar{c}_{\mathrm{avg,med}} = 2.5 \times 10^{-3} \text{ and}$$
$$Pe_{\mathrm{med}} = 9.54 \quad \text{and} \quad r = 2.85 \times 10^{-4}\ \mathrm{s}^{-1}$$
$$\text{for the case } \bar{c}(L_{\mathrm{med}}/2) = 2.5 \times 10^{-3}$$

Consequently, the values of γ_{med} will be $\gamma_{\mathrm{med}} = 1.1745 \times 10^{-1}$ and $\gamma_{\mathrm{med}} = 1.3401 \times 10^{-1}$. The calculated values of Pe_{med} and γ_{med} compare well with the values $Pe_{\mathrm{med}} \sim 4.4$ and $\gamma_{\mathrm{med}} \sim 8 \times 10^{-2}$ from the experimental measurements and computational analysis of Tedqui and Lever [40], Yuan et al. [35], Huang et al. [31]. Although the calculated values of k are relatively large compared to the value of $k = 1.4 \times 10^{-4}\ \mathrm{s}^{-1}$ provided by Morris et al. [46] and Truskey [42], it provides a good approximation for the concentration profile in the media as shown in Fig. 4(a).

If we specify the volume-averaged concentration $\bar{c}_{\mathrm{adv}} = 1.2 \times 10^{-2}$ at the media/adventitia interface based on the experimental data of Meyer et al. [34], the results will be

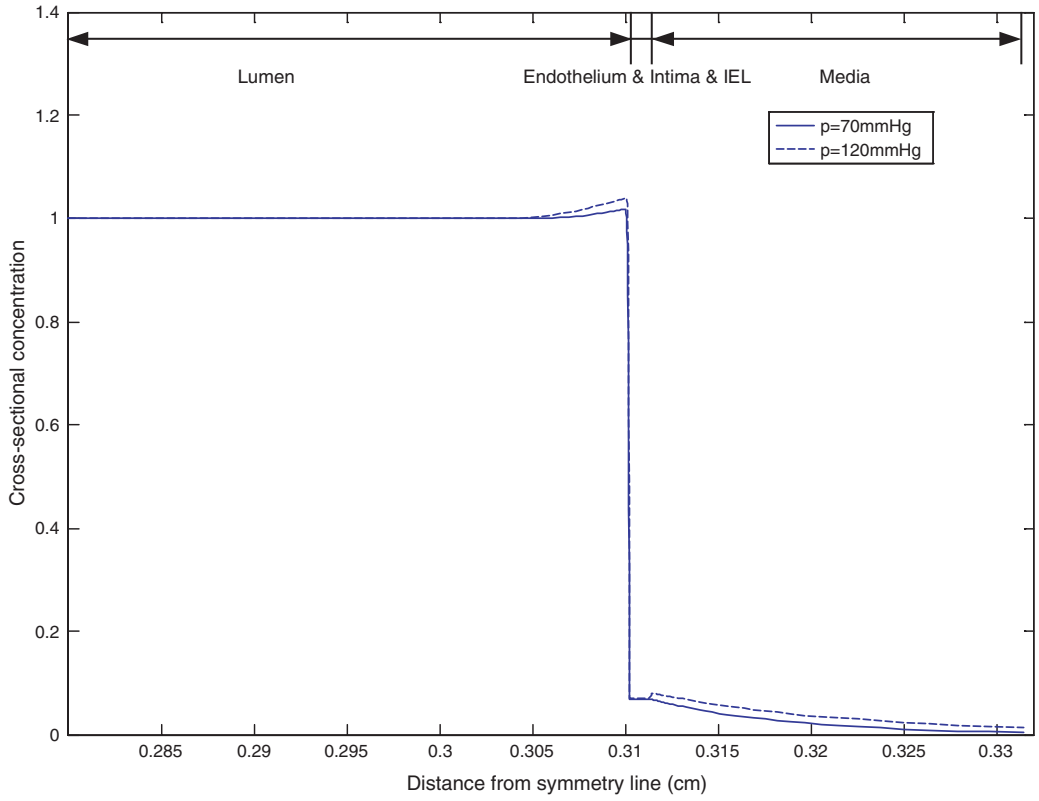

Fig. 11. Cross-sectional concentration profile.

$Pe_{\text{med}} = 5.77$ and $k = 6.71 \times 10^{-4}\ \text{s}^{-1}$ for the case $\bar{c}_{\text{avg,med}} = 2.5 \times 10^{-3}$ and $Pe_{\text{med}} = 9.52$ and $k = 2.86 \times 10^{-4}\ \text{s}^{-1}$ for the case $\bar{c}(L_{\text{med}}/2) = 2.5 \times 10^{-3}$

Consequently, the values of γ_{med} will be $\gamma_{\text{med}} = 8.1093 \times 10^{-2}$ and $\gamma_{\text{med}} = 1.3371 \times 10^{-1}$. From Fig. 4(b), it is obvious that the second case has a better agreement with the published data.

4.5. Determination of $D_{eff,iel}$

From the values obtained from the prior section, we can also obtain the concentration gradient at the IEL/media interface with the concentration profile given by Eq. (33).

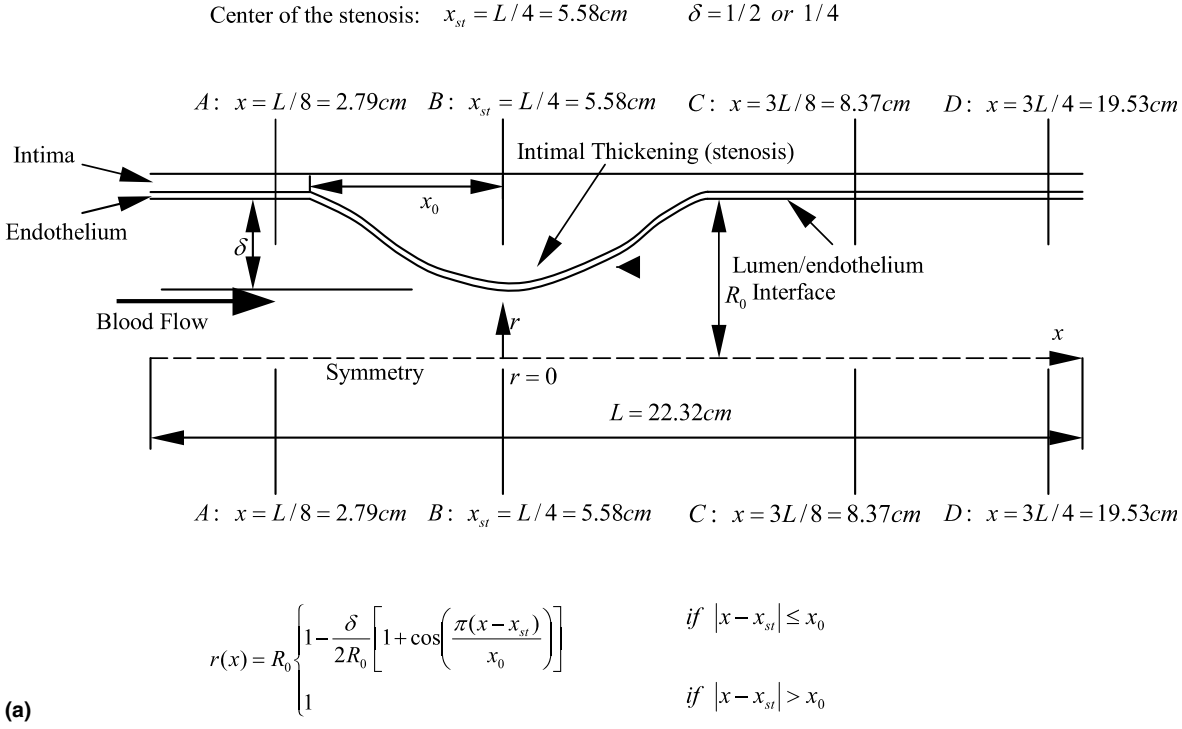

Fig. 12. (a) Geometry of constricted tube (upstream). (b) Geometry of constricted tube (downstream).

The matching conditions for the concentration gradients at the IEL/media interface can be given by

$$\nabla c^{+}_{\mathrm{med}} = \nabla c^{-}_{\mathrm{iel}} = \frac{\left(c^{-}_{\mathrm{iel}} - c^{+}_{\mathrm{iel}}\right)\lambda_{\mathrm{iel}} \mathrm{e}^{\lambda_{\mathrm{iel}} L_{\mathrm{iel}}}}{\mathrm{e}^{\lambda_{\mathrm{iel}} L_{\mathrm{iel}}} - 1} \tag{47}$$

The constant mass flux should be satisfied at relevant interfaces, which gives

$$N''_{\mathrm{s}} = -D_{\mathrm{eff,iel}} \nabla c^{+}_{\mathrm{iel}} + \gamma_{\mathrm{iel}} u \cdot n c^{+}_{\mathrm{iel}} \tag{48}$$

$$N''_{\mathrm{s}} = -D_{\mathrm{eff,int}} \nabla c^{+}_{\mathrm{int}} + \gamma_{\mathrm{int}} u \cdot n c^{+}_{\mathrm{int}} \tag{49}$$

These equations can also be rewritten in terms of the Peclet numbers for intima and IEL, Pe_{int} and Pe_{iel}. By realizing that $c^{+}_{\mathrm{iel}} = c^{-}_{\mathrm{int}}$ and $c^{-}_{\mathrm{iel}} = c^{+}_{\mathrm{med}}$, we have a nonlinear equation system for c^{-}_{int} and Pe_{iel}, Eqs. (50) and (51).

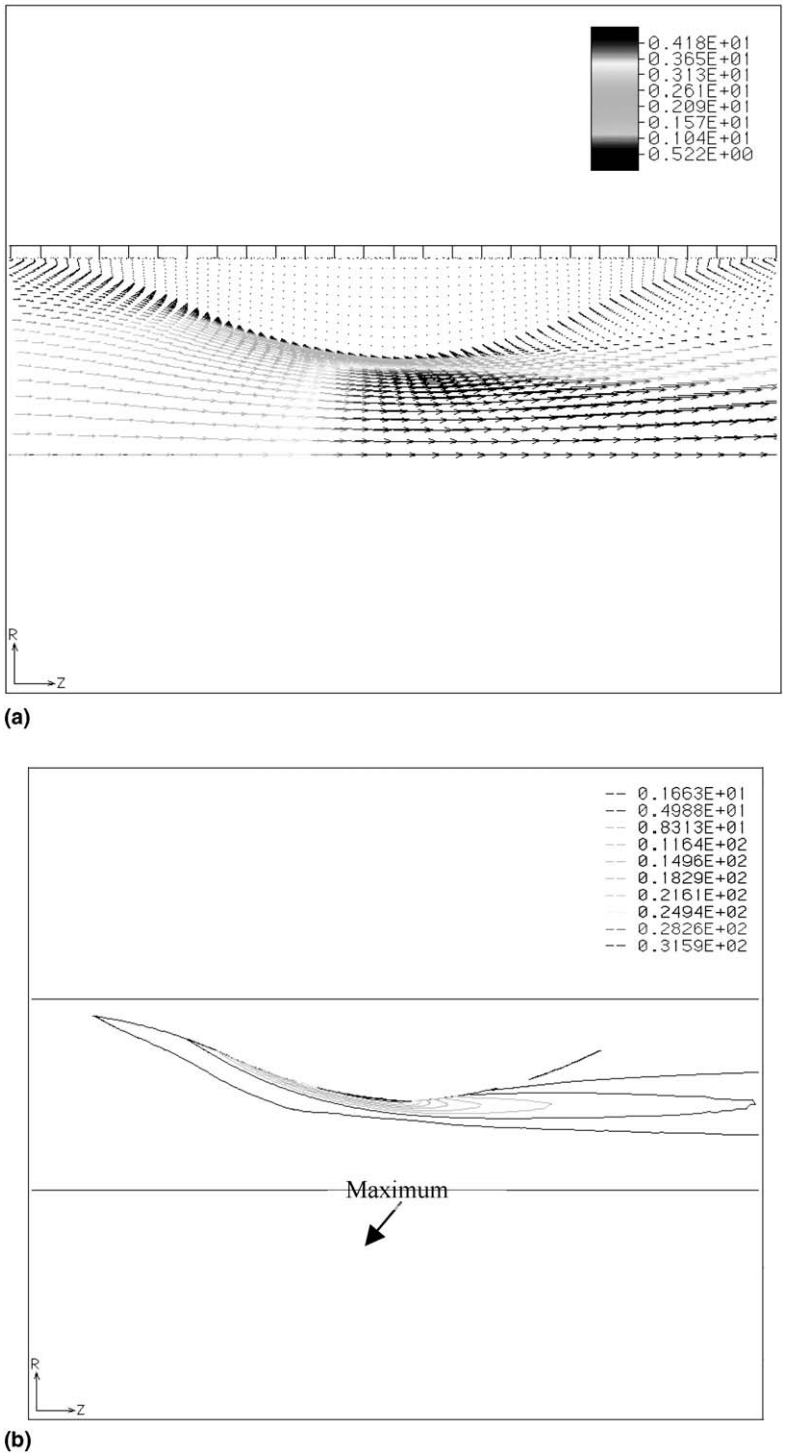

Fig. 13. (a) Velocity vectors near the stenosis ($x_{\mathrm{st}} = 5.58$ cm, $\delta = 1/2$). (b) Shear rate near the stenosis ($x_{\mathrm{st}} = 5.58$ cm, $\delta = 1/2$).

$$\nabla c^{-}_{\mathrm{iel}} = \frac{(c^{+}_{\mathrm{med}} - c^{-}_{\mathrm{int}})Pe_{\mathrm{iel}}e^{Pe_{\mathrm{iel}}}}{L_{\mathrm{iel}}(e^{Pe_{\mathrm{iel}}} - 1)} = \nabla c^{+}_{\mathrm{med}} \tag{50}$$

$$N''_{\mathrm{s}} = -D_{\mathrm{eff,iel}}\frac{(c^{+}_{\mathrm{med}} - c^{-}_{\mathrm{int}})Pe_{\mathrm{iel}}}{L_{\mathrm{iel}}(e^{Pe_{\mathrm{iel}}} - 1)} + \frac{Pe_{\mathrm{iel}}D_{\mathrm{eff,iel}}}{L_{\mathrm{iel}}}c^{-}_{\mathrm{int}}$$
$$= \frac{D_{\mathrm{eff,iel}}Pe_{\mathrm{iel}}(e^{Pe_{\mathrm{iel}}}c^{-}_{\mathrm{int}} - c^{+}_{\mathrm{med}})}{L_{\mathrm{iel}}(e^{Pe_{\mathrm{iel}}} - 1)} \tag{51}$$

To solve this system, we need to determine the effective diffusivity for the IEL layer. The available data for calculating the diffusivity of IEL are as follows:

(i) The diffusive permeability ratio of endothelium to IEL is $\kappa = 6.289 \times 10^{-5}$ obtained by Prosi et al. [10] from pore theory.
(ii) The diffusive permeability provided by Karner et al. [7] is $P_{\mathrm{diff,iel}} = 1.59 \times 10^{-7}$ cm/s, based on the pore theory.
(iii) The diffusive permeabilities obtained by Prosi et al. [10] are $P_{\mathrm{diff,end}} = 2.000126 \times 10^{-8}$ cm/s and $P_{\mathrm{diff,iel}} = 3.18 \times 10^{-4}$ cm/s based on the assumption of no convection.

Based on the definition of the diffusive permeability of the IEL $P_{\mathrm{diff,iel}} = \frac{D_{\mathrm{eff,iel}}}{L_{\mathrm{iel}}}$, we can calculate the values of diffusivity from the above three cases and obtain three different values for $D_{\mathrm{eff,iel}}$, namely, 6.5267×10^{-9} cm^2/s, 3.18×10^{-11} cm^2/s and 6.36×10^{-8} cm^2/s. These display a large deviation. It can be reasoned that the permeability values of Prosi et al. [10] which correspond to the endothelium diffusivity order of 10^{-12} cm^2/s are not accurate, based on our earlier analysis. It should be noted that the endothelium diffusivity order of 10^{-12} cm^2/s corresponds to $Pe_{\mathrm{end}} \sim 1$ which is not consistent with the experimental data.

We can evaluate the order of $D_{\mathrm{eff,iel}}$ by dividing Eq. (50) by Eq. (51). This results in

$$\frac{D_{\mathrm{eff,iel}}(c^{+}_{\mathrm{med}} - c^{-}_{\mathrm{int}})e^{Pe_{\mathrm{iel}}}}{D_{\mathrm{eff,iel}}\left(e^{Pe_{\mathrm{iel}}}c^{-}_{\mathrm{int}} - c^{+}_{\mathrm{med}}\right)} = \frac{D_{\mathrm{eff,iel}}\nabla c^{+}_{\mathrm{med}}}{N''_{\mathrm{s}}} \tag{52}$$

We can then rewrite the above equation as

$$\frac{-D_{\mathrm{eff,iel}}\nabla c^{+}_{\mathrm{med}}}{N''_{\mathrm{s}}} = 1 - \frac{c^{+}_{\mathrm{med}}(1 - e^{Pe_{\mathrm{iel}}})}{e^{Pe_{\mathrm{iel}}}c^{-}_{\mathrm{int}} - c^{+}_{\mathrm{med}}} \tag{53}$$

It is obvious that $Pe_{\mathrm{iel}} > 0$ which leads to

$$\frac{-D_{\mathrm{eff,iel}}\nabla c^{+}_{\mathrm{med}}}{N''_{\mathrm{s}}} < 1 \tag{54}$$

Based on the values of $\nabla c^{+}_{\mathrm{med}}$ and N_{s} from our previous analysis, we obtain $D_{\mathrm{eff,iel}} < 9.4 \times 10^{-10}$ cm^2/s for the largest concentration gradient value calculated at the IEL/media interface. As such, the value $D_{\mathrm{eff,iel}} = 3.18 \times 10^{-11}$ cm^2/s provided by Karner et al. [7] looks more reasonable. It results in a sieving coefficient for IEL $\gamma_{\mathrm{iel}} = 1.7048 \times 10^{-1}$ and a Peclet number of $Pe_{\mathrm{iel}} = 1.9$. This value is larger than the value obtained by Karner

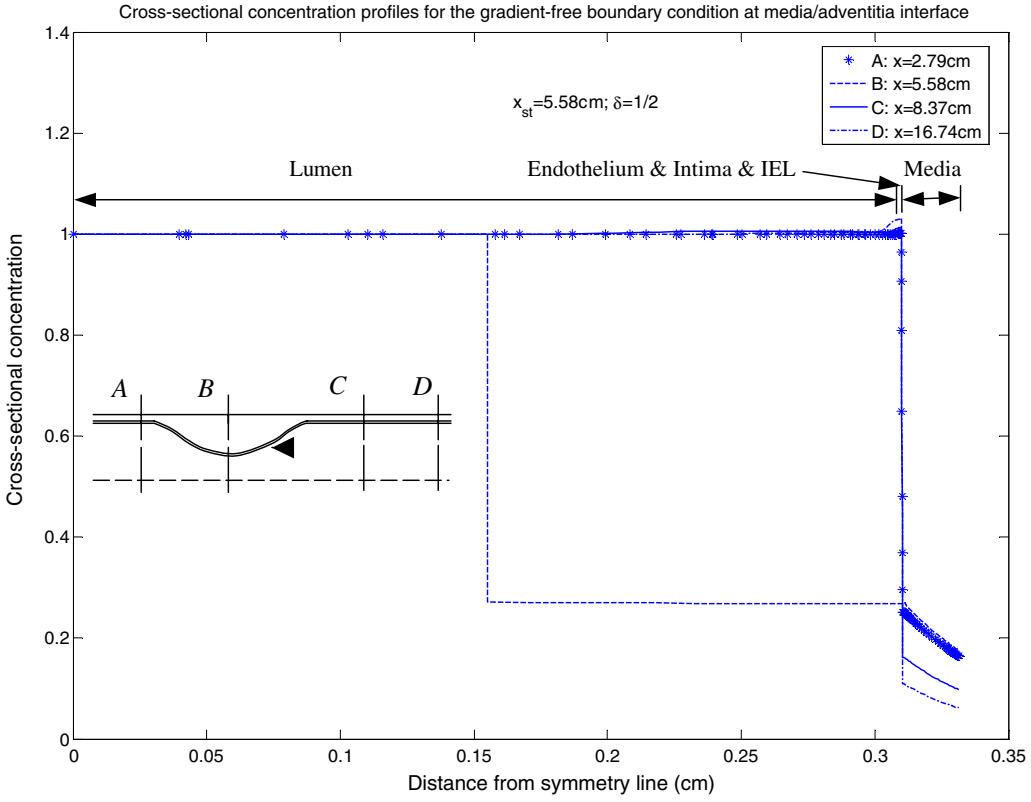

Fig. 14. Cross-sectional concentration profiles at different locations ($x_{\mathrm{st}} = 5.58$ cm, $\delta = 1/2$).

et al. [7] which is $\gamma_{iel} = 1.93 \times 10^{-2}$ based on the pore theory. But the calculated ratio between the sieving coefficients for endothelium and IEL is

$$\xi = \frac{\gamma_{end}}{\gamma_{iel}} = 6.735 \times 10^{-2} \tag{55}$$

which compares well with the published results [7,10].

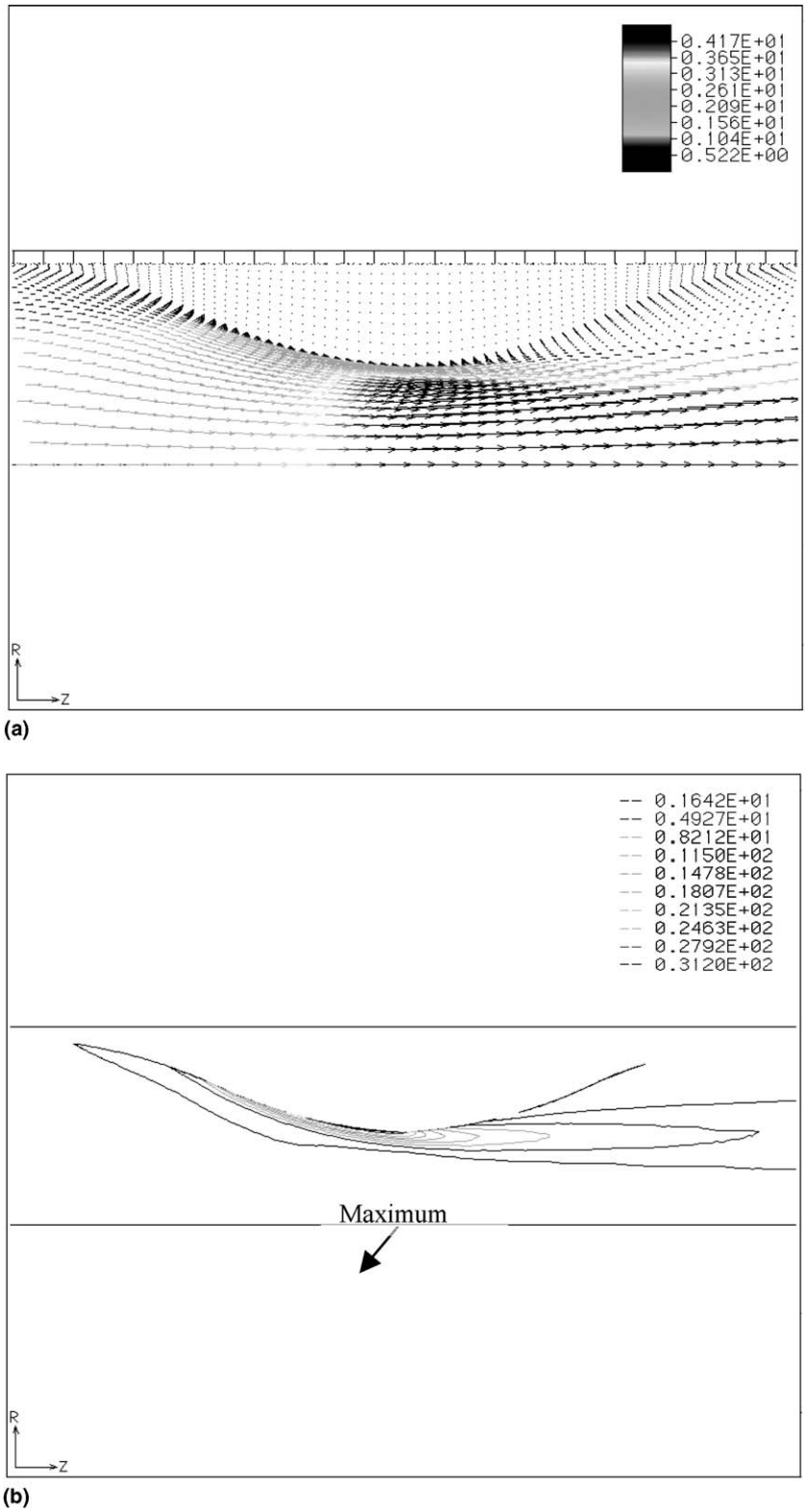

Fig. 15. (a) Velocity vectors near the stenosis ($x_{st} = 16.74$ cm, $\delta = 1/2$). (b) Shear rate near the stenosis ($x_{st} = 16.74$ cm, $\delta = 1/2$).

From our numerical analysis, we find that the boundary condition we choose at the media/adventitia interface has a small effect on the calculated value of γ_{iel} and c^-_{int}. With the parameter values $D_{eff,iel} = 3.18 \times 10^{-11}$ cm^2/s and $\gamma_{iel} = 1.7048 \times 10^{-1}$, the calculated concentration at the intima/IEL interface is $c^-_{int} = 6.749 \times 10^{-2}$. Due to the large diffusivity for the intima $D_{eff,int} = 5.0 \times 10^{-8}$ cm^2/s, it can be seen from Eq. (49) that the concentration drop across the intima is negligible. As such, we can neglect the diffusive resistance and rewrite Eq. (49) as

$$N''_s = \gamma_{int} u \cdot n c^-_{int} \tag{56}$$

This results in

$$\gamma_{int} = \frac{N''_s}{u \cdot n c^-_{int}} = 0.17084 \tag{57}$$

which compares well with the values proposed by Huang et al. [31] ($\gamma_{int} = 1.99 \times 10^{-2}$–$1.536 \times 10^{-1}$) and Prosi et al. [10] ($\gamma_{int} = 1.727709 \times 10^{-1}$). As such the Peclet number we obtain is $Pe_{int} = 6.1 \times 10^{-3}$, which indicates diffusion is the dominant species transport mode within the intima. The complete set of the constants and parameters used in the current model are listed in Table 2.

Numerical results agree well with the analytical solutions for each layer as shown in Figs. 5 and 6. Fig. 7 shows the concentration obtained at all the interfaces with the gradient-free boundary condition. Fig. 8 shows a good agreement between the numerical results with two different boundary conditions and the experimental data.

5. Effects of the hypertension

It is well known that systemic arterial hypertension has a significant impact on the process of atherogenesis. Three factors are proposed to explain the contribution of hypertension to atherogenesis. The first is that the increased transmural pressure causes an increase in the transmural fluid flux, which leads to a greater convective mass flux. The second is that an increased fluid flux enhances the concentration polarization developed at the lumen/endothelium interface, which in turn increase the mass flux in two ways. One is that the higher concentration at interface increases the total mass flux if the permeability is assumed to stay unchanged. The other one is that the higher concentration at the interface may even increase the wall permeability itself. The third factor is that the permeability of the wall may be pressure dependent [8].

We assume that all the wall parameters remain unchanged under the increased transmural pressure. The transmural pressure is increased from 70 mm Hg to 120 mm Hg. An increase of transmural pressure greatly elevates the filtration velocity as shown in Fig. 9. The effects of transmural pressure on the concentration polarization are shown in Fig. 10, which shows that the hypertension substantially increases the concentration at

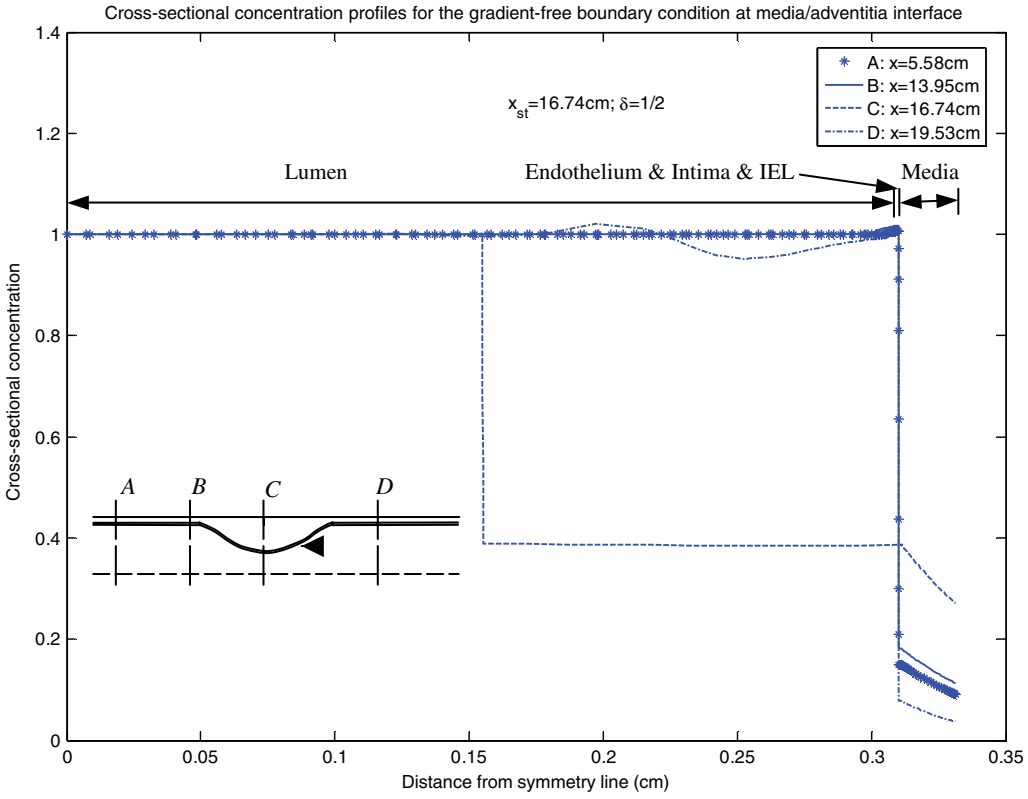

Fig. 16. Cross-sectional concentration profiles at different locations ($x_{st} = 16.74$ cm, $\delta = 1/2$).

the lumen/endothelium interface. The cross-sectional concentration profiles under both pressure conditions are shown in Fig. 11. From Fig. 11, it can be seen that the concentration in the media layer is increased noticeably while the concentration increases slightly in the intima layer.

6. Effects of the stenosis

The physical parameters computed in the previous sections are used to study the effects of stenosis. A further validation is needed for the current model being applied to

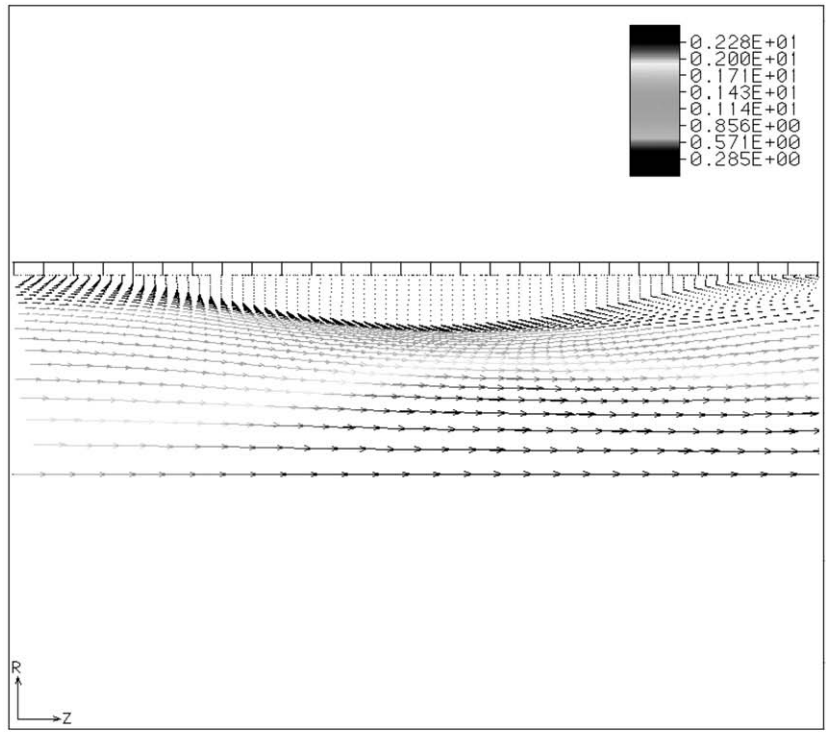

(a)

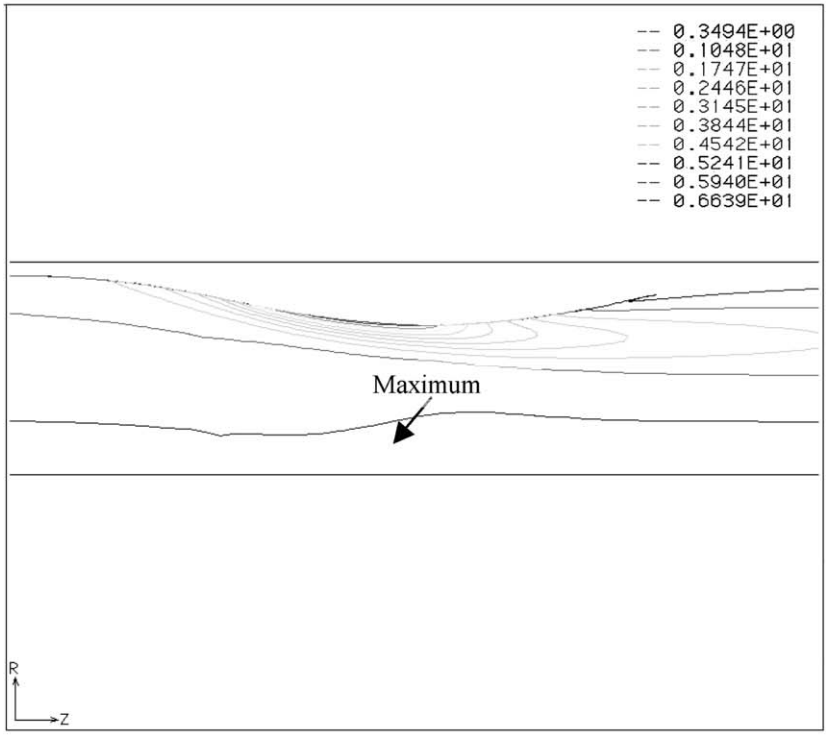

(b)

Fig. 17. (a) Velocity vectors near the stenosis ($x_{st} = 5.58$ cm, $\delta = 1/4$). (b) Velocity vectors near the stenosis ($x_{st} = 5.58$ cm, $\delta = 1/4$).

vascular regions more complex than a straight tube. Particular interest exists in studying the axi-symmetric stenotic artery which corresponds to an artery wall which is either constricted or the intima layer is thickened. Intimal thickening is mainly caused by SMC proliferation inside the vessel wall.

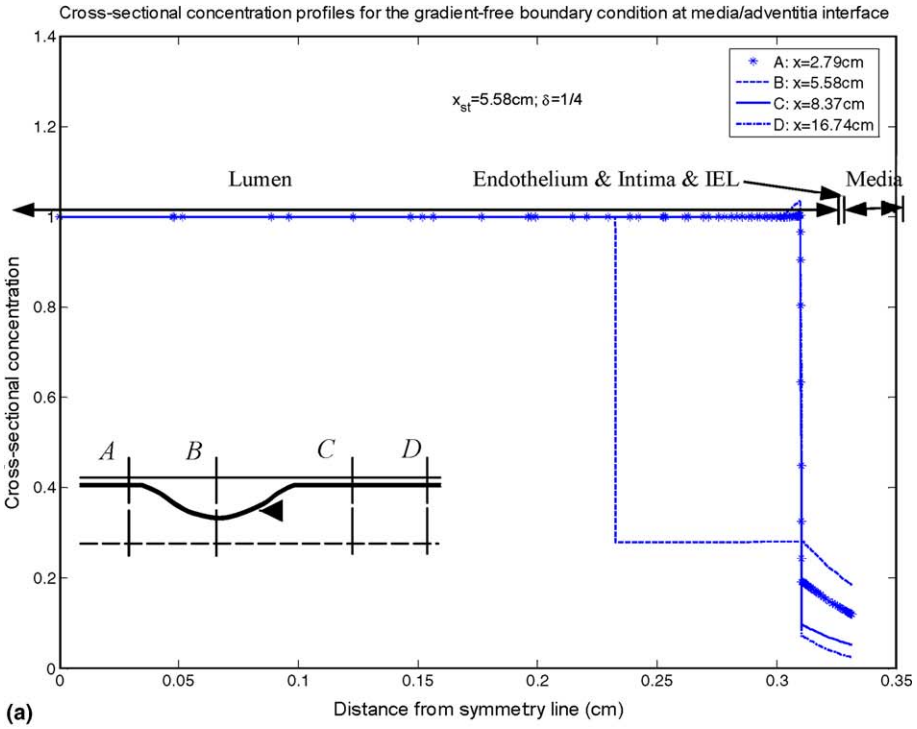

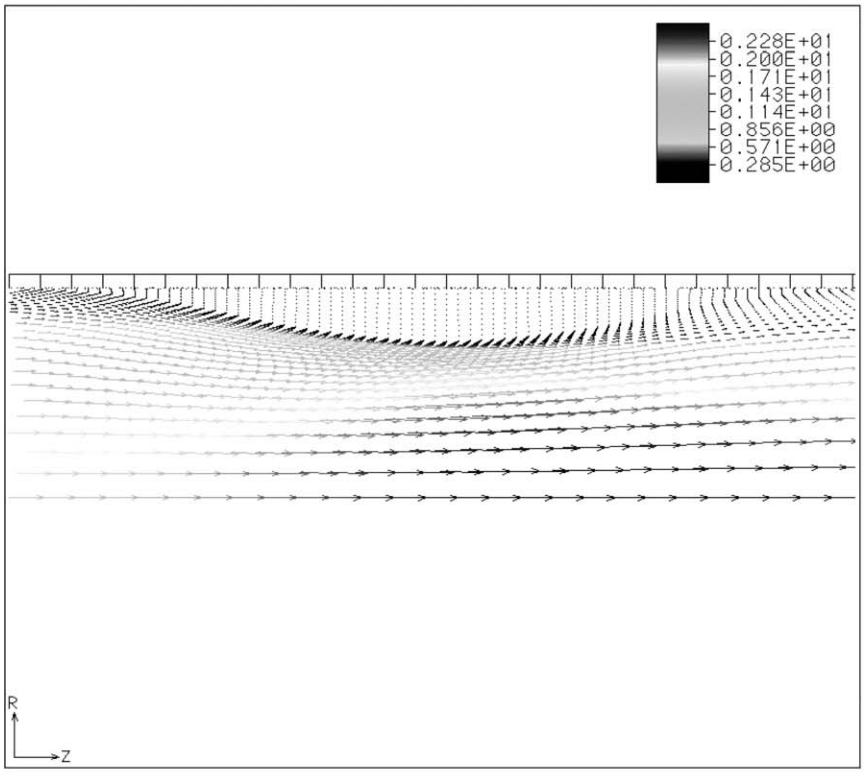

Fig. 18. (a) Cross-sectional concentration profiles at different locations ($x_{st} = 5.58$ cm, $\delta = 1/4$). (b) Velocity vectors near the stenosis ($x_{st} = 16.74$ cm, $\delta = 1/4$).

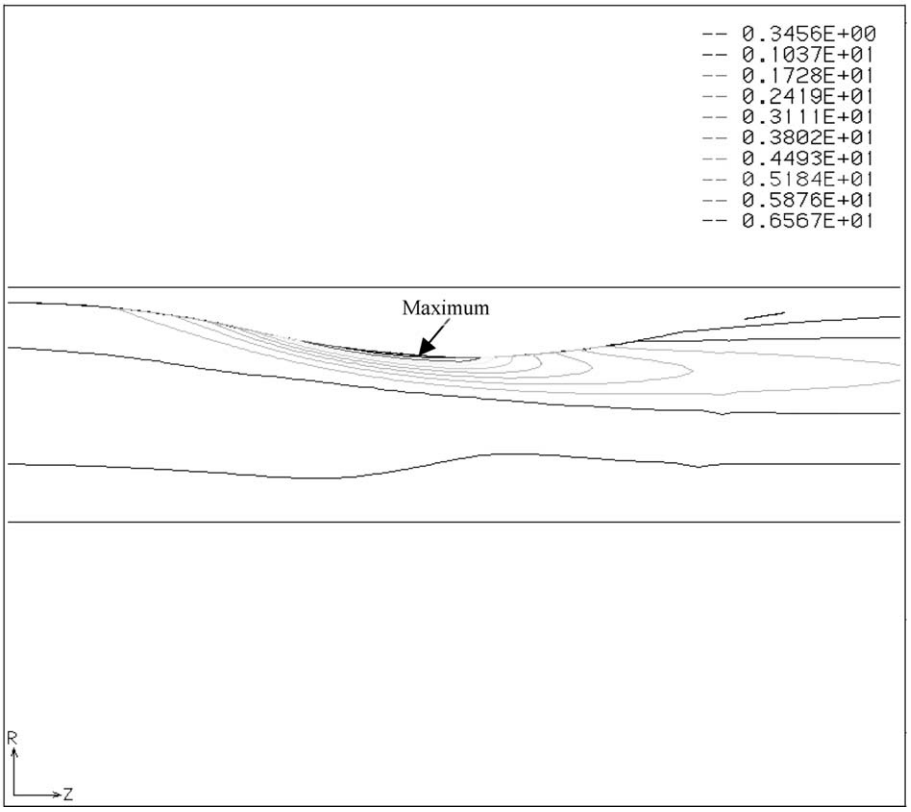

Fig. 19. Shear rate near the stenosis ($x_{st} = 16.74$ cm, $\delta = 1/4$).

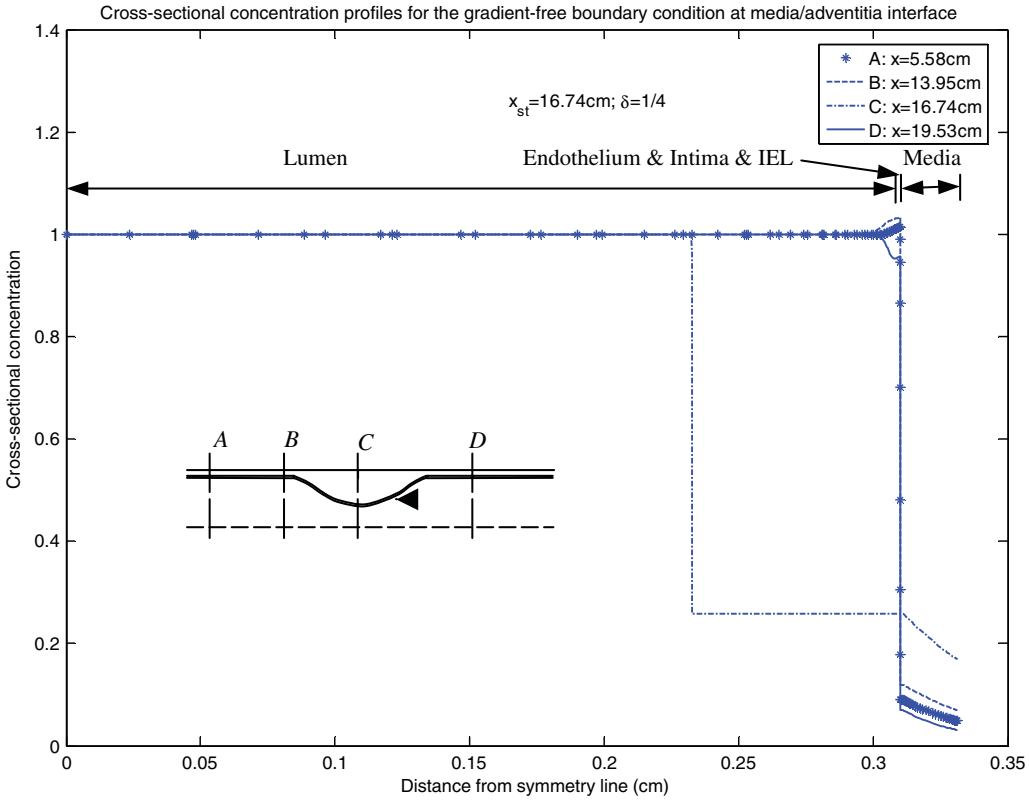

Fig. 20. Cross-sectional concentration profiles at different locations ($x_{st} = 16.74$ cm, $\delta = 1/4$).

As shown in Fig. 12(a) and (b), the tubular geometry is determined by the radius R_0 and the local, smooth axi-symmetric constriction [47]

$$r(x) = R_0 \begin{cases} 1 - \frac{\delta}{2}\left[1 + \cos\left(\frac{\pi(x - x_{st})}{x_0}\right)\right], \\ \quad \text{if } |x - x_{st}| \leqslant x_0 \\ 1, \quad \text{if } |x - x_{st}| > x_0 \text{ and } 0 \leqslant x \leqslant L_{st} \end{cases} \tag{58}$$

where x_{st} is the x coordinate of the center of the stenosis, x_0 is the stenosis half-length, L_{st} is the total length of vessel with stenosis and δ is the dimensionless thickness of the luminal reduction in the radial direction. We choose $x_0 = 2R_0 = 0.62$ cm, $L_{st} = 72R_0 = 22.32$ cm.

The definition of area reduction A_{red} is given by

$$A_{red} = 1 - \left(\frac{r(x_{st})}{R_0}\right)^2 = 1 - (1 - \delta)^2 \tag{59}$$

Classifications of stenoses were first given by the World Health Organization [48] in three specified luminal narrowing grades [49]:

No stenosis: No reduction in the area of the arterial lumen.

Moderate stenosis: More than half of the original lumen diameter remaining ($A_{red} < 75\%$).

Severe stenosis: Less than half the original lumen diameter remaining ($A_{red} > 75\%$).

From the fluid mechanical point of view, severe stenosis reductions may induce turbulence, high wall shear stresses, and greatly vary shear stress gradients. From a physiological standpoint, it is believed that the fluid mechanics will trigger either greater luminal thickening or for a particle cluster of the stenosis to shear off leading directly to thrombi formation followed by emboli possibly leading to a heart attack or stroke [49].

We take the dimensionless thickness of the luminal reduction in the radial direction as $\delta = 1/2$ and $\delta = 1/4$, which implies 75% (severe occlusion) and 43.75% (moderate occlusion) area reduction respectively.

The effects of stenosis are studied at two different locations $x_{st} = \frac{L_{st}}{4}$ and $x_{st} = \frac{3L_{st}}{4}$, as shown in Fig. 12(a) and (b). The results obtained from this study are shown in Figs. 13–20, from which it can be seen that the stenoses has pronounced effects on the velocity field and the wall concentration. As shown in Figs. 13(a), 15(a), 17(a) and 18(b), the maximum velocity vector appears slightly after the throat and then starts to decrease. From Figs. 13(b), 15(b), 17(b) and 19, it can be seen that the maximum shear rate occurs on the stenosis slightly before the throat. The shear rate also starts to decrease after the throat. The concentration profiles are obtained at four different places (Fig. 12(a) and (b)) depending on the location of the stenosis, as shown in Figs. 14, 16, 18(a) and 20. From these figures, it can be seen that the occurrence of stenosis greatly perturbs the species distribution inside the wall. The wall species concentration near the region of stenosis is increased dramatically. The wall concentration approaches to its unperturbed value shortly after the stenosis.

7. Conclusion

A new model based on the porous media theory and experimental data is proposed in the current study. The results of the new model represent physical transport process of LDL in the blood stream and inside the artery wall. It is shown that hypertension greatly increases the transmural filtration and concentration polarization at the lumen/endothelium interface. The effects of the stenosis on the velocity and concentration fields are analyzed. The maximum shear rate appears before the throat while the velocity vector reaches its maximum value slightly after the throat. The wall concentration is greatly increased near the region of stenosis and approaches its unperturbed value shortly after the stenosis.

References

[1] K. Khanafer, K. Vafai, K. Kangarlu, Computational modeling of cerebral diffusion-application to stroke imaging, Magn. Reson. Imaging 21 (2003) 651–661.
[2] K. Khanafer, K. Vafai, K. Kangarlu, Water diffusion in biomedical systems as related to magnetic resonance imaging, Magn. Reson. Imaging 21 (2003) 17–31.
[3] M. Yang, X. Zhang, K. Vafai, C. Ozkan, High sensitivity piezoresistive cantilever design and optimization for analyte-receptor binding, J. Micromech. Microeng. 13 (2003) 864–872.
[4] K. Khanafer, A.-R.A. Khaled, K. Vafai, Spatial optimization of an array of aligned microcantilever biosensors, J. Micromech. Microeng. 14 (2004) 1328–1336.
[5] A.-R.A. Khaled, K. Vafai, Optimization modeling of analyte adhesion over an inclined microcantilever-based biosensors, J. Micromech. Microeng. 14 (2004) 1220–1229.
[6] A.-R.A. Khaled, K. Vafai, Analysis of oscillatory flow disturbances and thermal characteristics inside fluidic cells due to fluid leakage and wall slip conditions, J. Biomech. 37 (2004) 721–729.
[7] G. Karner, K. Perktold, H.P. Zehentner, Computational modeling of macromolecule transport in the arterial wall, Comput. Methods Biomech. Biomed. Eng. 4 (2001) 491–504.
[8] D.K. Stangeby, C.R. Ethier, Computational analysis of coupled blood-wall arterial LDL transport, J. Biomech. Eng. 124 (2002) 1–8.
[9] P. Zunino, Mathematical and numerical modeling of mass transfer in the vascular system, Ph.D. thesis, Ecole Polythéchnique Fédérale de Lausanne, (2002).
[10] M. Prosi, P. Zunino, K. Perktold, A. Quarteroni, Mathematical and numerical models for transfer of low-density lipoproteins through the arterial walls: a new methodology for the model set up with applications to the study of disturbed luminal flow, J. Biomech. 38 (2005) 903–917.
[11] S. Wada, T. Karino, Computational study on LDL transfer from flowing blood to arterial walls, in: T. Yamaguchi (Ed.), Clinical Application of Computational Mechanics to the Cardiovascular System, Springer, 2000, pp. 157–173.
[12] D. Fry, Mathematical models of arterial transmural transport, Am. J. Physiol. 248 (2) (1985) 240–263.
[13] L. Ai, K. Vafai, An investigation of Stokes' second problem for non-Newtonian fluids, Numer. Heat Transfer, Part A 47 (2005) 955–980.
[14] K. Vafai, C.L. Tien, Boundary and inertia effects on flow and heat transfer in porous media, Int. J. Heat Mass Transfer 24 (1981) 195–203.
[15] B. Alazmi, K. Vafai, Analysis of variants within the porous media transport models, ASME J. Heat Transfer 122 (2000) 303–326.

[16] A.-R.A. Khaled, K. Vafai, The role of porous media on modeling flow and heat transfer in biological tissues, Int. J. Heat Mass Transfer 46 (2003) 4989–5003.
[17] B. Alazmi, K. Vafai, Analysis of variable porosity, thermal dispersion, and local thermal non-equilibrium on free surface flows through porous media, ASME J. Heat Transfer 126 (2004) 389–399.
[18] J.B. Butt, Reaction Kinetics and Reactor Design, second ed., Marcel Dekker, New York, 1999.
[19] S. Liu, J.H. Masliyah, in: K. Vafai (Ed.), Handbook of Porous Media, second ed., CRC Press, Taylor & Francis, 2005, pp. 81–140.
[20] A. Amiri, K. Vafai, Analysis of dispersion effects and non-thermal equilibrium non-Darcian, variable porosity incompressible flow through porous medium, Int. J. Heat Mass Transfer 37 (1994) 939–954.
[21] O. Kedem, A. Katchalsky, Thermodynamic analysis of the permeability of biological membranes to non-electrolytes, Biochem. Biophys. Acta 27 (1958) 229–245.
[22] F. Curry, in: E.M. Renkin (Ed.), Handbook of Physiology, American Physiological Society, Bethesda, MD, 1984.
[23] W.M. Deen, Hindered transport of large molecules in liquid-filled pores, AIChE J. 33 (9) (1987) 1409–1425.
[24] H. Jo, R.O. Dull, T. Hollis, J. Tarbell, Endothelial albumin permeability is shear dependent, time dependent and reversible, Am. J. Physiol. 260 (1991) 1992–1996.
[25] D. Wang, J. Tarbell, Modelling interstitial flow through arterial media allows estimation of wall shear stress on smooth muscle cells, Trans ASME J. Biomech. Eng. 117 (1995) 358–363.
[26] C.C. Michel, F. Curry, Microvascular permeability, Physiol. Rev. 79 (3) (1999) 703–761.
[27] FIDAP Theoretical Manual, Evanston, IL: Fluid Dynamics International, 1990.
[28] K. Vafai, R. Thiyagaraja, Analysis of flow and heat transfer at the interface region of a porous medium, Int. J. Heat Mass Transfer 30 (1987) 1391–1405.
[29] J. Tarbell, M. Lever, C. Caro, The effect of varying albumin concentration and hydrostatic pressure on hydraulic conductivity of the rabbit common carotid artery, Microvasc. Res. 35 (1988) 204–220.
[30] Y. Huang, S. Weinbaum, S. Rumschitzki, D. Chien, A fiber matrix model for the growth of macromolecular leakage spots in the arterial intima, ASME Adv. Biol. Heat Mass Transfer HTD-231 (1992) 81–92.
[31] Y. Huang, S. Rumschitzki, D. Chien, S. Weinbaum, A fiber matrix model for the growth of macromolecular leakage spots in the arterial intima, J. Biomech. Eng. 116 (1994) 430–445.
[32] Y. Hunag, Y. Rumschizki, D. Chien, S. Weinbaum, A fiber matrix model for the filtration through fenestral pores in a compressible arterial intima, Am. J. Physiol. 272 (1997) 2023–2039.
[33] G. Trusky, W. Roberts, R. Herrmann, R. Malinauskas, Measurement of endothelial permeability to ^{125}I-low density lipoproteins in rabbit arteries by use of en face preparations, Circ. Res. 7 (4) (1992) 883–897.
[34] G. Meyer, R. Merval, A. Tedgui, Effects of pressure stretch and convection on low-density lipoprotein and albumin uptake in the rabbit aortic wall, Circ. Res. 79 (3) (1996) 532–540.
[35] F. Yuan, S. Chien, S. Weinbaum, A new view of convective–diffusive transport processes in the arterial intima, ASME J. Biomech. Eng. 113 (1991) 314–329.
[36] M. Whale, A. Grodzisky, M. Johnson, The effect of aging and pressure on the specific hydraulic conductivity of the aortic wall, Biorheology 33 (1996) 17–44.
[37] J. Tarbell, M. Lever, C. Caro, The effect of varying albumin concentration and hydrostatic pressure on hydraulic conductivity of the rabbit common carotid artery, Research 35 (1988) 204–220.
[38] R. Dull, H. Jo, H. Still, T. Hollis, J. Tarbell, The effect of varying albumin concentration and hydrostatic pressure on hydraulic conductivity and albumin permeability of cultured endothelial monolayers, Microvasc. Res. 41 (1991) 390–407.
[39] X. Deng, Y. Marois, T. How, Y. Merhi, M. King, R. Guidoin, T. Karino, Luminal surface concentration of lipoprotein (LDL) and its effect on the wall uptake of cholesterol by canine carotid arteries, J. Vasc. Surg. 21 (1995) 135–145.
[40] A. Tedgui, M.J. Lever, The interaction of convection and diffusion in the transport of ^{131}I-Albumin within the media of rabbit thoracic aorta, Circ. Res. 57 (1985) 856–863.
[41] S. Tada, J.M. Tarbell, Internal elastic lamina affects the distribution of macromolecules in the arterial wall: a computational study, Am. J. Physiol. Heart Circ. Physiol. 287 (2004) 905–913.
[42] G. Trusky, Low density lipoprotein transport and metabolism in the arterial wall, Ph.D. Thesis, Cambridge: Massachusetts Institute of Technology, 1985.
[43] N. Yang, K. Vafai, Modeling of low-density lipoprotein (LDL) transport in the artery—effects of hypertension, Int. J. Heat Mass Transfer 49 (2006) 850–867.
[44] J.M. Tarbell, Mass transport in arteries and the localization of atherosclerosis, Annu. Rev. Biomed. Eng. 5 (2003) 79–118.
[45] Z.J. Huang, J.M. Tarbell, Numerical simulation of mass transfer in porous media of blood vessel walls, Am. J. Physiol Heart Circ. Physiol. 273 (1997) H464–H477.
[46] E. Morris, G. Saidel, G.M. Chisolm, Optimal design of experiments to estimate LDL transport parameters in arterial wall, Model. Physiol. (1991) 929–949.
[47] D.F. Young, Fluid mechanics of arterial stenosis, J. Biomech. Eng. 101 (1979) 157–175.
[48] World Health Organization, WHO Technical Report Series, No. 143. Geneva: WHO, 1958.
[49] J.R. Buchanan, Computational analysis of particle-hemodynamics in stenosed artery segments, M.S. Thesis, Raleigh: North Carolina State University, 1996.